MODELS FOR PREDICTING THE NO_X EXHAUST POLLUTANTS IN A DIESEL ENGINE

Diploma Paper
by
Petra Andersson
LRAP – 96 (1989)
Department of Physics Lund
together with
Saab – Scania Södertälje

CONTENTS

INTRODUCTION

The diesel combustion process is very complex and it is difficult to foretell what the effects of a change in, for example, engine geometry might be. Thus the improvement of diesel engines is time–consuming since the commonly used approach is to alter the engine and then test it. Much work has been done in recent years in on attempt to develop models for diesel combustion.

This paper presents the results of a literature search on models that predict the NO_x exhaust in diesel engines. The databases searched through are: SAE, COMPENDEX, NTIS, CEA and CHEMABS.

Nine models were found and are presented in order of increasing model refinement. At the end of the paper a number of different approaches to decreasing NO_x exhaust are presented.

References referred to are [1] –[56]. References [57] –[73] have been studied but are not referred to and are listed for the sake of completeness.

1 NO_x FORMATION

Since NO is the major component in combustion and NO_2 is formed from it upon reaching the atmosphere, models of NO_x formation focus on NO formation.[3] In fig.1 we can see the equilibrium concentration of nitrogen oxide versus temperature in air.

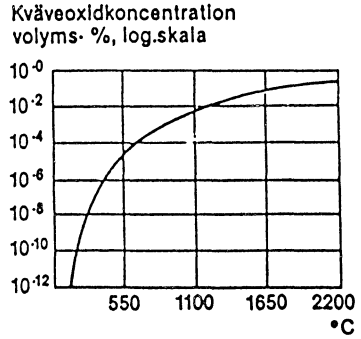

Fig. 1. Nitrogen oxide equilibrium concentration versus temperature.

Fortunately, the combustion process is much faster than the NO formation so we never obtain the equilibrium concentration. There are three ways of forming NO:

thermal NO
prompt NO
fuel NO.

1:1 THERMAL NO

Thermal NO is formed via the Zeldovich mechanism [2]

$$O + N_2 \rightleftarrows NO + N \quad k=1.4\cdot10^{14}\exp(-78500/RT) \tag{1}$$

$$N + O_2 \rightleftarrows NO + O \quad k=6.4\cdot10^{9}\exp(-6280/RT) \tag{2}$$

where k is the forward rate constant. A third reaction contributes in fuel–rich flames

$$N + OH \rightleftarrows NO + H \quad k=2.8\cdot10^{13} \tag{3}$$

Reactions (1)–(3) are called the extended Zeldovich mechanism. Reaction (1) has a high activation energy and controls the mechanism. Since reaction (1) is slow, thermal NO is formed in the postflame region.

Initially, and often throughout the high–temperature part of the process, the NO concentration is much less than its equilibrium value so the reverse of reactions (1) and (2) can be neglected. If we neglect reaction (3) and suppose O to be in equilibrium with O_2,

then we obtain a nitric oxide formation rate given by [7]

$$\frac{d[NO]}{dt} = 10^{15.6}\, T^{-1} \exp(-68400/T) \cdot [N_2] \cdot [O_2]^{1/2} \cdot P^{1/2} s^{-1} \qquad (4)$$

where T is the temperature in K and P is the pressure in atm.

Often one cannot assume atomic oxygen to be equilibrated with oxygen. Schefer and Sawyer [14] obtained formula (7) assuming equations (5) and (6) to be equilibrated.

$$CO + OH \rightleftharpoons CO_2 + H \qquad (5)$$

$$H + O_2 \rightleftharpoons OH + O \qquad (6)$$

$$\frac{d[NO]}{dt} = 2k_{1f}K_5K_6\frac{[N_2][CO][O_2]}{[CO_2]} \qquad (7)$$

where k_{1f} is the forward rate constant of reaction (1) and K_5 and K_6 are the equilibrium constants of reactions (5) and (6), respectively. Mass fractions of O_2 and CO were computed from O, H and C atom concentrations. The agreement was fair when the formula was tested on an opposed reacting jet using propane as fuel. In fig. 2 a comparision between the NO formation rate obtained using eqs. (4) and (7) is made. In eq. (7) k_{1f} is taken from the rate data of Baulch et al.[55], $k_{1f} = 7.6 \cdot 10^{13} \exp(-38000/T)$, K_5 and K_6 are obtained by dividing the forward by the reverse rate constant taken from Gardiner [54], which gives $K_5 = 2.75 \cdot 10^{-8} T^{1.5} \exp(106.9/RT)$ and $K_6 = 6.67 \cdot 10^{4} T^{-0.91} \exp(-69.1/RT)$. Mole fractions of CO, O_2 and CO_2 were taken from measurements presented in [56], see fig. 2.

Thompson et al.[12] have suggested that since reactions (8) to (11) are fast they are assumed to be equilibrated and the thermal NO_x formation is expressed as (12)

$$H + O_2 \rightleftharpoons OH + O \qquad (8)$$

$$O + H_2 \rightleftharpoons OH + H \qquad (9)$$

$$H_2 + OH \rightleftharpoons H_2O + H \qquad (10)$$

$$OH + OH \rightleftharpoons H_2O + O \qquad (11)$$

$$\frac{d[NO]}{dt} = 2k_{1f}K_8K_{10}[H_2][O_2][N_2]/[H_2O] \qquad (12)$$

where k_{1f} is the forward rate constant of reaction (1) and K_8 and K_{10} are the equilibrium constants of reactions (8) and (10), respectively.

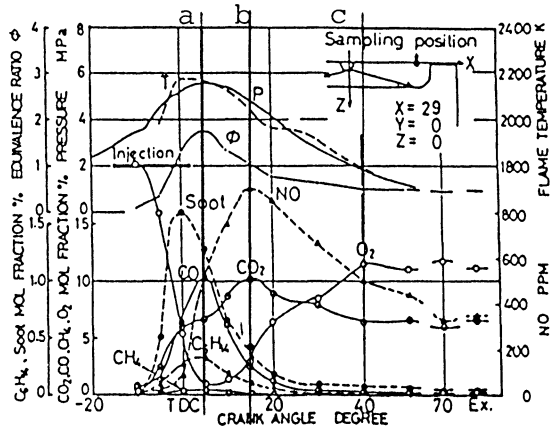

Fig. 2. Histories of local O_2, CO, CO_2 and other combustion products in a 4–stroke–DI–diesel engine with a displacement of 780 cc, bore·stroke = 95·110 mm, a compression ratio of 14.6 and 4 nozzle holes with ϕ = 0.2 mm. Operating conditions :1250 rpm, $\lambda = 1.8$, $\theta = -15^{\circ}$ATDC and $P_{inj} = 17$ MPa.

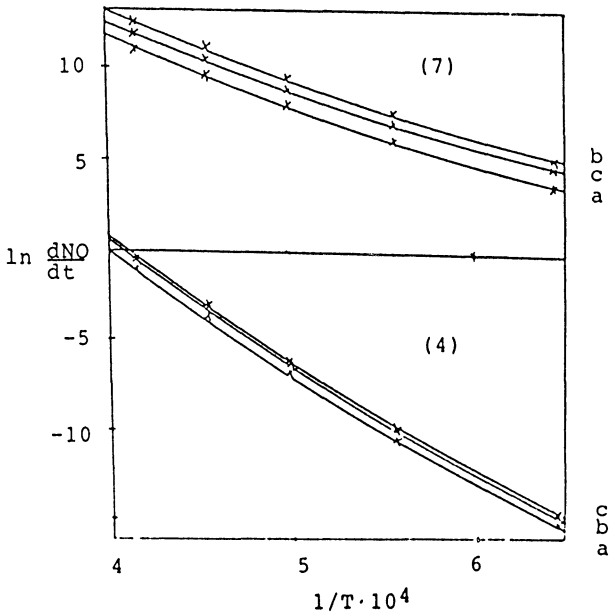

Fig. 3. Ln dNO/dt versus 1/T obtained from eq. (4) and eq. (7) and fig. 2.

If we only assume reaction (8) to be equilibrated and the nitrogen atom concentration to be at its steady–state value, the formation rate is given by [13]

$$\frac{d[NO]}{dt} = 2[O]\left[\frac{k_{f1}[N_2] - k_{r1}k_{r2}[NO]^2/k_{f2}[O_2]}{1+k_{r1}[NO]/(k_{f2}[O_2]+k_{f3}[OH])}\right] \qquad (13)$$

where k_f and k_r are the forward and reverse rate constants of reactions. The term $k_{f3}[OH]$ can be neglected in lean flames and [O] is assumed to have its equilibrium value. Fig.4 shows the strong temperature dependence of $[NO_x]$ due to the Zeldovich mechanism.[4]

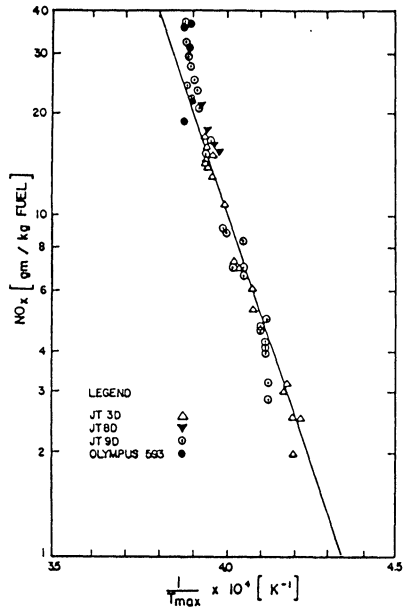

Fig. 4. Nitric oxide emissions from aircraft gas turbines presented in Arrhenius form. The prediction is based on Zeldovich kinetics and the assumption of equilibrium oxygen atom concentration at the adiabatic flame temperature for a stoichiometric mixture.

1:2 PROMPT NO

Fenimore [9] obtained axial [NO] profiles for premixed flat flames, extrapolated these profiles back to the burner head and found a rapid generation of NO in the reaction zone, which he named "prompt NO", see fig. 5. Many believed that this could be due to the O radical overshoot but no prompt NO is found in nonhydrocarbon flames; the Zeldovich mechanism is independent of fuel type. Prompt NO is weakly temperature dependent and more prompt NO is found in fuel–rich flames. Fenimore found that for a flame of ϕ=0.8 and P=1–3 bar, prompt NO varied approximately as $P^{1/2}$, which seems to rule out the [O] overshoot as the main cause of fast early NO formation, since higher pressures promote radical recombination. Hayhurst and Vince [3] found the reactions to be

$$CH + N_2 \rightarrow HCN + N \qquad (14)$$
$$CH_2 + N_2 \rightarrow HCN + NH \qquad (15)$$

where N in reaction (11) can yield NO by reaction (2), and HCN and NH form NH_i species through various reactions with O radicals. In the absence of hydrocarbons (that is in all but the richest hydrocarbon flames) NO and N_2 are formed via the reactions

$$NI + O_x \rightarrow NO + \ldots \quad (16)$$

$$NI' + NO \rightarrow N_2 + \ldots \quad (17)$$

where NI and NI′ are nitrogenous intermediates consisting of one or more NH_i species and O_x is an oxygen–containing species. 90% of the prompt NO formation is due to the HCN reactions with O radicals. In very rich flames the prompt exactly is not completely as above.

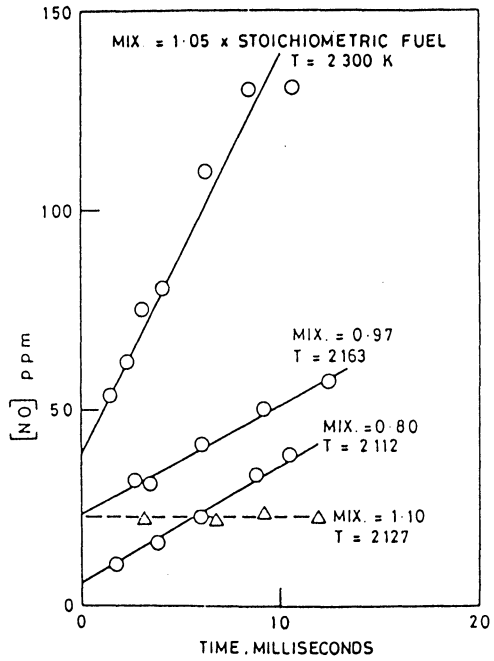

Fig. 5. Measured [NO] along four ethylene–air flames as a function of reaction time; i.e. the distance of the point of sampling from the burner face divided by the calculated velocity of the burned gases. The mixture strength and temperature of each flame are as quoted. Mix is the equivalence ratio.

Bachmaier et al. [10] measured the prompt NO formation as a function of equivalence ratio for many hydrocarbon compounds. Fig. 6 shows the results where we can see that the maximum prompt NO content is reached on the fuel–rich side and drops off sharply at an equivalence ratio of about 1.4.[2]. Bachmaier et al. also measured the HCN concentrations through propane–air flames. These results, which can be found in fig. 7, show that the HCN concentration rises sharply somewhere in the flame and then decreases sharply. But for the equivalence ratio of 1.5 it continues to rise. Little prompt NO is found for ϕ=1.5. The explanation for this is that HCN is formed in all the rich hydrocarbon flames but below ϕ=1.4 there are still enough O radicals present to react with HCN and form NO.

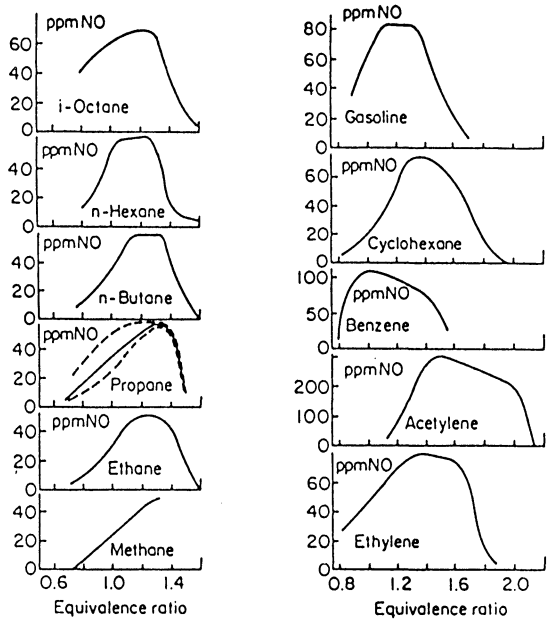

Fig. 6. "Prompt NO" as a function of mixture strength and fuel. Dotted lines show the uncertainty of the extrapolation for the determination of prompt NO in propane flames, similar curves were obtained for the other hydrocarbons.

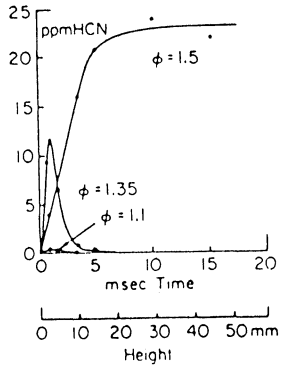

Fig.7. HCN profiles of fuel–rich propane–air flames.

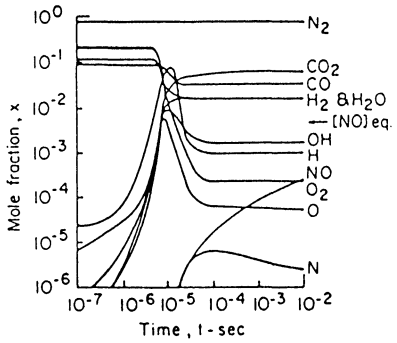

Fig. 8. Concentration–time profiles in the kinetic calculation of the methane–air reaction with an inlet temperature of 1000 K, P_{in}=10 atm, ϕ=1.0 and T_c=2477 K

Fig. 8 shows a large oxygen radical overshoot within the reaction zone that can lead to prompt NO found in flames due to the Zeldovich mechanism. Eberius and Just (1973) measured the prompt NO in the flame zone at various equivalence ratios and flame temperatures; the results are shown in fig. 9. The results indicate that there are two mechanisms for the formation of prompt NO. Nowadays prompt NO is defined as that nitric oxide which results from N_2 via reactions other than the Zeldovich mechanism. [1]

De Soete [8] has given an empirical equation for the rate of prompt NO production

$$\frac{d[NO]}{dt}\Big|_{prompt} = k_c\,[O_2]^b[N_2]\,[fuel]\,\exp(-E_a/RT) \qquad (18)$$

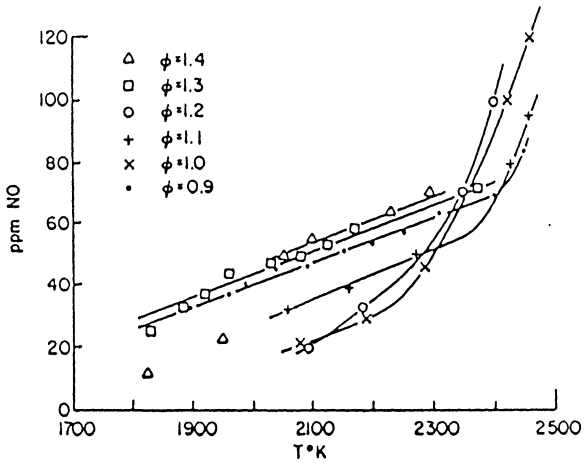

Fig.9. Prompt NO as a function of the temperature at various mixture strengths ϕ in adiabatic propane–synthetic air flames.

The table below [3] shows how much NO_x is due to prompt NO, as can be seen, not very much NO_x in a diesel engine is formed via the prompt mechanism.

Table 1. Emission factors for nitrogen oxides; the role of prompt NO. The conversion factors are; 1 ft^3 = 28.32 l, 1 lb = 0.45 kg and 1 gallon = 3.78 l.

Source	Average emission factor (as NO_2)	% estimated due to prompt NO
Natural gas:		
household and commercial	116 lb/million ft^3 gas burned	57
industry	214 lb/million ft^3 gas burned	31
utility	390 lb/million ft^3 gas burned	17
Gas engines	770–7300 lb/million ft^3 gas burned	2–21
Gas turbines	200 lb/million ft^3 gas burned	30
Gasoline-powered motor vehicle	113 lb/1000 gal. fuel	10
Diesel engine	222 lb/1000 gal. fuel	5

1:3 FUEL NO

Fuel NO results from nitrogen compounds bound in the fuel, e.g. [11]:

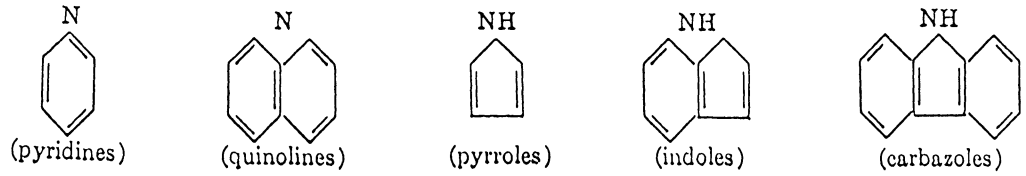

These compounds are believed to pyrolyze or react to form an intermediate nitrogen–containing species I, (HCN or NH_i, i=0,1,2,3), reaction (19). I can react with an oxygen–containing molecule R to form NO, reaction (20) or with NO or another I to form N_2, reaction (21).

$$\text{fuel nitrogen} \rightarrow \text{I} \tag{19}$$

$$\text{I} + \text{R} \rightarrow \text{NO} \tag{20}$$

$$\text{I} + \begin{bmatrix} \text{NO} \\ \text{I} \end{bmatrix} \rightarrow \text{N}_2 \tag{21}$$

Once the intermediate is formed the fuel NO formation is very much like the Fenimore prompt NO mechanism. Fuel NO formation is rapid, slightly dependent on temperature and sensitive to the fuel–air ratio. More fuel NO is obtained on the lean side of stoichiometric.

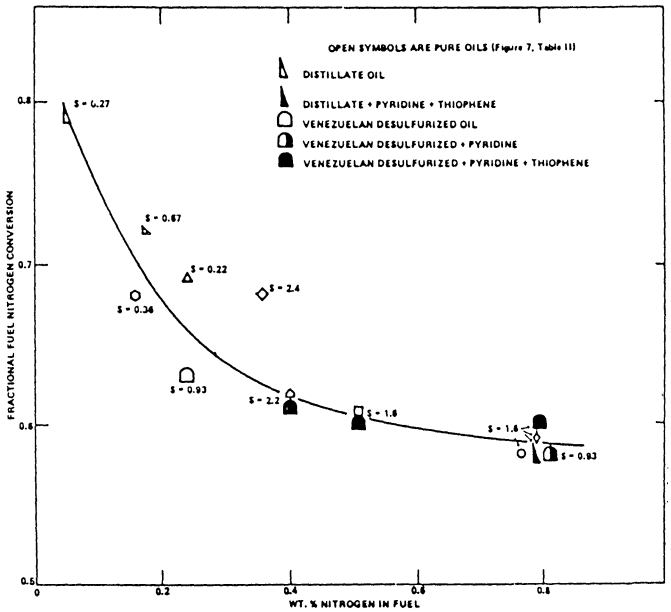

Fig. 10. Fractional fuel nitrogen conversion versus weight % nitrogen in fuel for synthetic oils.

Fig. 10 shows the inverse relationship between the fraction of fuel nitrogen converted to nitric oxide and the percentage of nitrogen in the fuel.[5]

De Soete [8] has proposed a formula for the formation of fuel NO

$$k_a[\text{fuel–N}][O_2]\exp(-E_a/RT) \tag{22}$$

where k_a and E_a depend on the nature of the fuel nitrogen and the mixture strength.

2 DIESEL ENGINES

There are two types of diesel engines, Direct Injected (DI) and InDirect Injected (IDI) diesel engines. IDI diesel engines have a prechamber. During the intake process in a diesel engine air is drawn in while the combustion chamber (in a IDI the main chamber) is expanded. Near Bottom Dead Centre (BDC) the intake valve is closed and the air is then compressed, causing the temperature to rise. Before Top Dead Centre (TDC) high–pressure fuel injection through a nozzle commerces. When, at any location, the fuel–air mixture and temperature are right, auto–ignition occurs. Thus the combustion process in a diesel engine is very complex; at some locations the fuel burns and at others the fuel may still be in the liquid phase. After a while the exhaust valve opens and lets out the exhaust. The exhaust valve is then closed and the cycle begins again.

3 MODELS

In fig. 11 the models discussed in this paper are presented schematically. The models formulated to predict NO_x formation in a diesel engine can be separated into three different groups; models that do not take into consideration physical and chemical aspects, models that treat the combustion chamber as a well–stirred reactor and models that treat the combustion chamber as a partially stirred reactor. The first group called "regression models", is presented with the necessary input data. Input data are divided into three groups, calculated, measured and geometrical. In some models, the "measured" data may be estimated or assumed to have a certain value. For the "well–stirred" group the chemistry considered is also presented. The "partially stirred" group is presented with "degree of heterogeneity", how the mixing in the chamber is treated, chemistry and input data.

3:1 REGRESSION MODELS

The simplest way to formulate a model is to postulate an equation dependent on choosen parameters and then select values of constants in the equation to fit experimental results. Callahan et al.[15] have developed such an emission model for effects of discrete transients in speed and load. They obtained

$$\text{Emission} = \prod_{i=0}^{14} \exp(b_i x_i) \tag{23}$$

where b_i and x_i are given in table 3. Table 2 explains S_i, T_i, t and t_s. The constants b_i are given for a four–cylinder Caterpillar 3304 engine with a precombustion chamber. It has a bore of 12.07 cm, stroke 15.24 cm, a total displacement of 6.9 litres and with a compression ratio of 17.5:1 it has a rated power of 58 kW at 1800 rpm. In fig. 12 the transient test cycle used is shown.

Table 2. Summary of the independent variables which define an individual segment.

Variable	Description	Range
S_0	Beginning Speed Preceding Segment	(0.33-1.0)
S_1	Beginning Speed	(0.33-1.0)
S_2	Ending Speed	(0.33-1.0)
T_0	Beginning Torque Preceding Segment	(0.05-1.0)
T_1	Beginning Torque	(0.05-1.0)
T_2	Engine Torque	(0.05-1.0)
t	Segment Length	(3.0-12.)
t_s	Length of Preceding Segment (sec)	(3.0-12.)

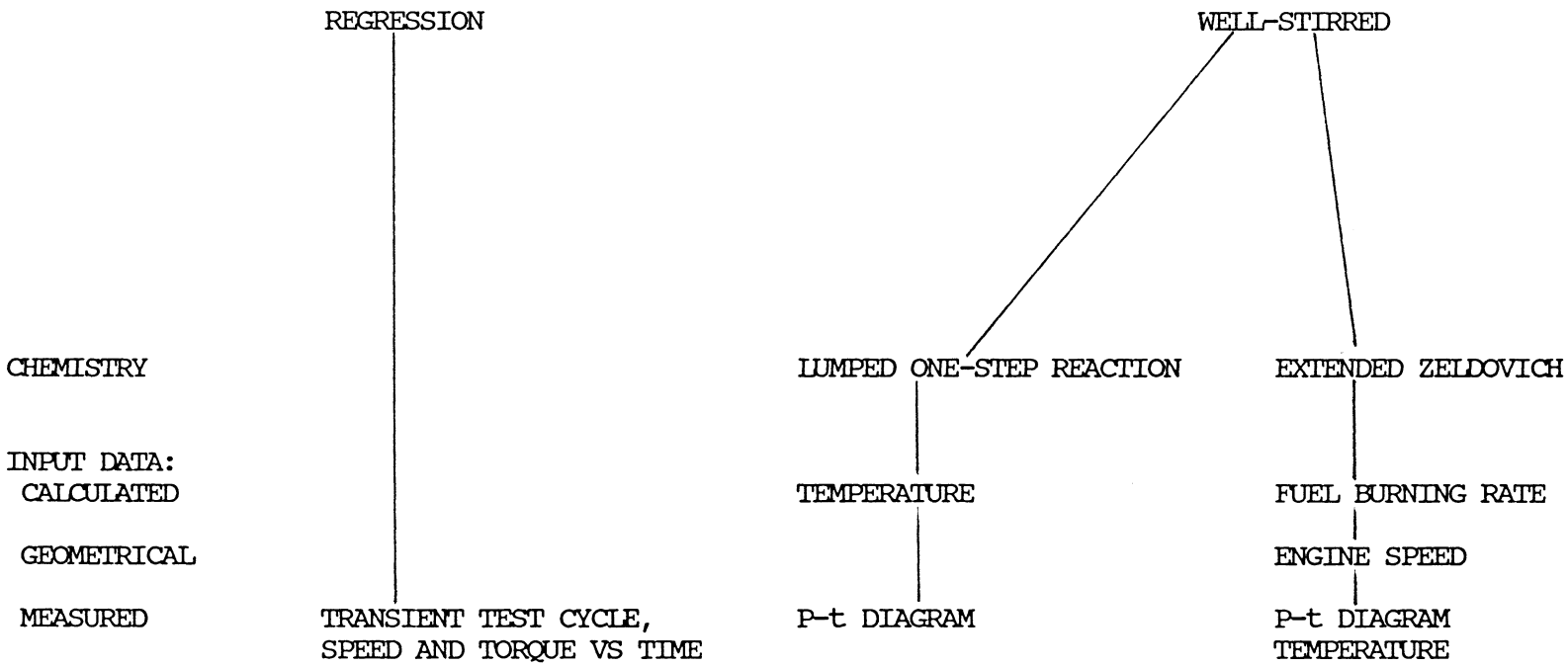
REGRESSION
WELL-STIRRED
CHEMISTRY
LUMPED ONE-STEP REACTION
EXTENDED ZELDOVICH
INPUT DATA:
CALCULATED
TEMPERATURE
FUEL BURNING RATE
GEOMETRICAL
ENGINE SPEED
MEASURED
TRANSIENT TEST CYCLE,
SPEED AND TORQUE VS TIME
P-t DIAGRAM
P-t DIAGRAM
TEMPERATURE

Fig. 11.

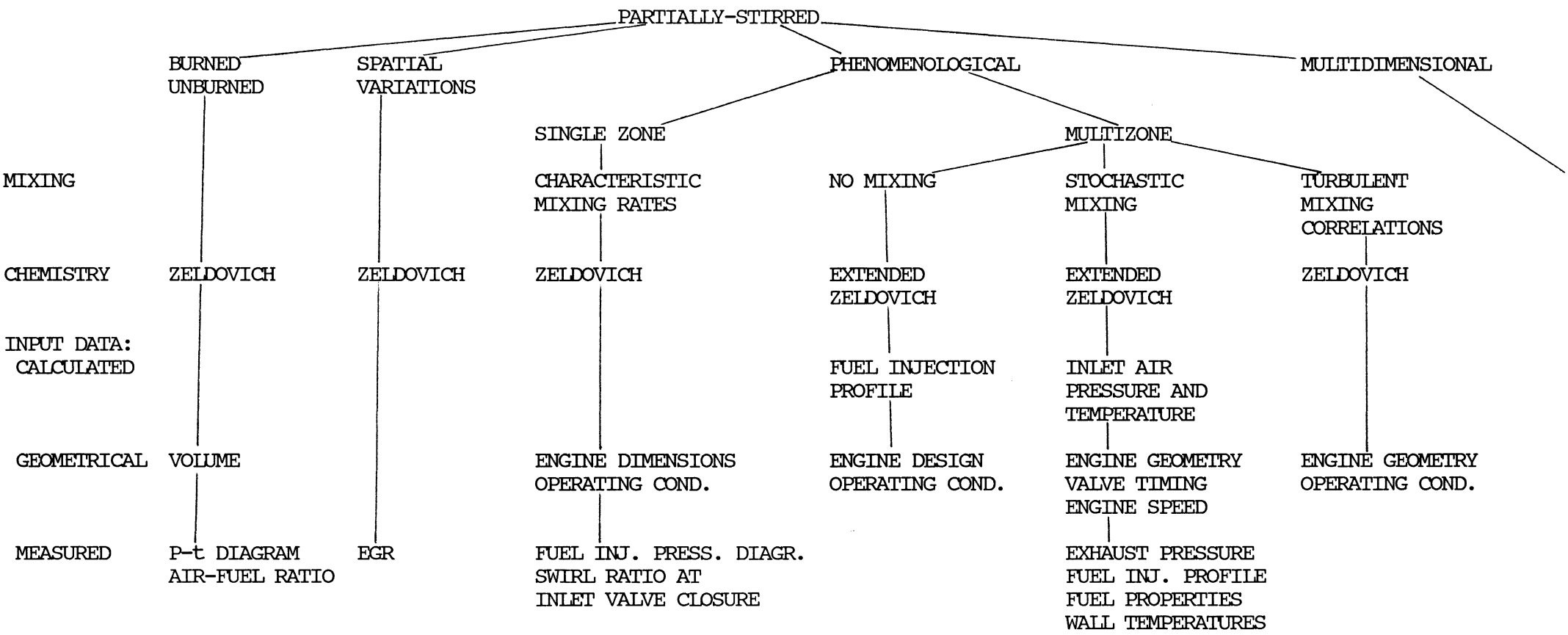
PARTIALLY-STIRRED
BURNED
UNBURNED
SPATIAL
VARIATIONS
PHENOMENOLOGICAL
MULTIDIMENSIONAL
SINGLE ZONE
MULTIZONE
MIXING
CHARACTERISTIC
MIXING RATES
NO MIXING
STOCHASTIC
MIXING
TURBULENT
MIXING
CORRELATIONS
CHEMISTRY
ZELDOVICH
ZELDOVICH
ZELDOVICH
EXTENDED
ZELDOVICH
EXTENDED
ZELDOVICH
ZELDOVICH
INPUT DATA:
CALCULATED
FUEL INJECTION
PROFILE
INLET AIR
PRESSURE AND
TEMPERATURE
GEOMETRICAL
VOLUME
ENGINE DIMENSIONS
OPERATING COND.
ENGINE DESIGN
OPERATING COND.
ENGINE GEOMETRY
VALVE TIMING
ENGINE SPEED
ENGINE GEOMETRY
OPERATING COND.
MEASURED
P-t DIAGRAM
AIR-FUEL RATIO
EGR
FUEL INJ. PRESS. DIAGR.
SWIRL RATIO AT
INLET VALVE CLOSURE
EXHAUST PRESSURE
FUEL INJ. PROFILE
FUEL PROPERTIES
WALL TEMPERATURES

Fig. 11.

Table 3. Definition of predictor variables used in the regression model and regression coefficients for the prediction of emission values.

X_i	Definition	Variable		EMISSION PART	NO_x	HC	CO
X_0	1	Intercept	B_0	-4.12051	-1.44556	-4.67497	-2.35942
X_1	$(S_1+S_2)/2$	S_{avg}	B_1	0.77846	2.23998	1.96005	0.94206
X_2	$(T_1+T_2)/2$	T_{avg}	B_2	3.12313	1.06198	1.82168	1.56467
X_3	$(.5-X_1)^2$	S_{avg}^2	B_3	1.50094	-1.89555	0.00000	0.00000
X_4	$(.5-X_2)^2$	T_{avg}^2	B_4	-0.95937	-3.70856	-0.74231	2.52417
X_5	$(.5-X_1)(.5-X_2)$	$S_{avg} \cdot T_{avg}$	B_5	-4.57653	0.58855	-2.27054	-1.90942
X_6	ln t	t	B_6	0.88636	1.08608	0.96030	1.02298
X_7	$(S_2-S_1)/t$	dS/dt	B_7	2.70045	2.86009	-0.81500	1.77668
X_8	$(T_2-T_1)/t$	dT/dt	B_8	0.51054	1.26178	-1.20295	1.45372
X_9	X_7^2	dS/dt^2	B_9	0.00000	-3.24582	0.00000	0.00000
X_{10}	X_8^2	dT/dt^2	B_{10}	5.55000	-3.57931	0.00000	5.22559
X_{11}	$(S_1-S_0)/t_s/t$	$dS_0/dt/t$	B_{11}	0.00000	-5.75900	-8.00259	0.00000
X_{12}	$(T_1-T_0)/t_s/t$	$dT_0/dt/t$	B_{12}	0.00000	0.00000	0.00000	0.00000
X_{13}	$(X_{11} \cdot 100)^2$	$(dS_0/dt/t)^2$	B_{13}	0.00000	0.00000	0.00000	0.00000
X_{14}	$(X_{12} \cdot 100)^2$	$(dT_0/dt/t)^2$	B_{14}	0.00000	0.02321	0.00000	0.00000
			r^2	0.8090	0.9611	0.9152	0.9081
			MSE	0.21179	0.03004	0.06456	0.06338

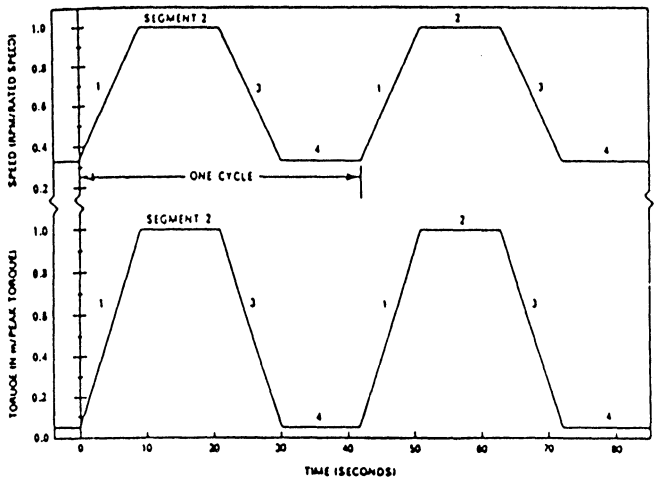

Fig. 12. Transient test cycles: speed and torque versus time.

3:2 WELL–STIRRED REACTOR

In a well–stirred reactor everything is spatially uniform. Here, two well–stirred models are presented, a "lumped one–step reaction" model and a model based on the extended Zeldovich mechanism.

3:2:1 LUMPED ONE–STEP REACTION

In refs [16] and [17] a correlation technique for flame temperature effects on NO_x for both direct ignition and divided chamber diesel engines is presented. For both engines the expression used is

$$EINO_x = C \exp(E/RT_f) \tag{24}$$

where $EINO_x$ is the NO_x emission index (g of NO_x as NO_2/kg fuel), C is a factor which depends upon flow characteristics, E is the overall activation energy (cal/mole), R is the gas constant (cal/mole K) and T_f is the stoichiometric adiabatic flame temperature. The flame temperatures were calculated at TDC using a version of the NASA equilibrium program. C is not determined but by letting $T_f \to \infty$ in fig. 13 we obtain $C = 1.6 \cdot 10^7$. From table 4 we can obtain values of E/R for NO_x, particulate carbon (C), volatiles (V) and gas–phase hydrocarbons (HC).

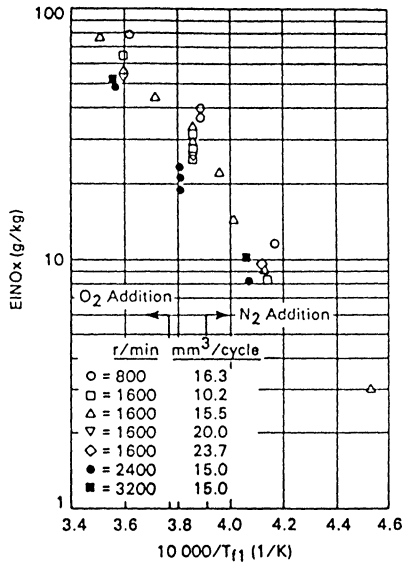

Fig. 13. Flame temperature correlation for NO_x emission index.

Table 4. Flame temperature correlations for divided–chamber dieselengines.

Emission Index (g/kg fuel)	E/R* (K) 0.72-L Engine	0.52-L Engine
EINOx	-36 700	-36 700
EIC	48 900	41 100
EIV	26 700	15 600
EIHC	15 100	9 600

Plee et al. [17] changed the flame temperature by increasing the amount of intake gas or by elevating the intake air temperature for different loads and speeds in two divided–chamber diesel engines, one with a displacement of 0.72 L/cyl and a low swirl prechamber, and one with a displacement of 0.52 L/cyl and a high swirl prechamber. They found that for temperatures higher than 2125 K the overall activation energy is constant for all operating conditions, as we can see in fig. 14, where normalized $EINO_x$ versus T_f is shown. The normalized $EINO_x$ is obtained by dividing $EINO_x$ at a given condition with $EINO_x$ for standard air for the same condition. By using the normalized $EINO_x$ the effect of C in (24) is omitted. This indicates that the effect of intake gas addition is primarly due to changes in temperature rather than to concentration changes, and that load and speed do not affect the temperature dependence. They also found that the chamber geometry did not affect the flame temperature dependence, as we can see in fig. 15.

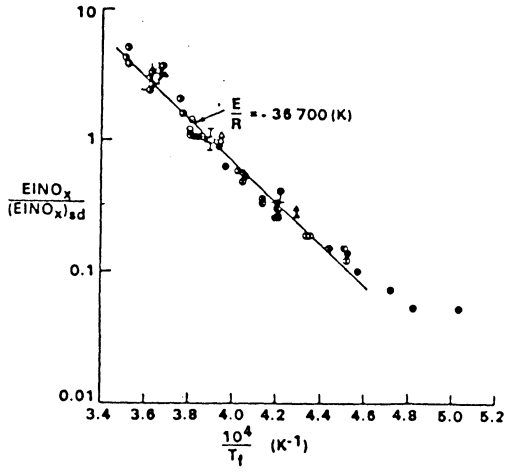

Fig. 14. Correlation of normalized $EINO_x$ with stoichiometric flame temperature for the 0.72 L diesel, all loads/speeds.

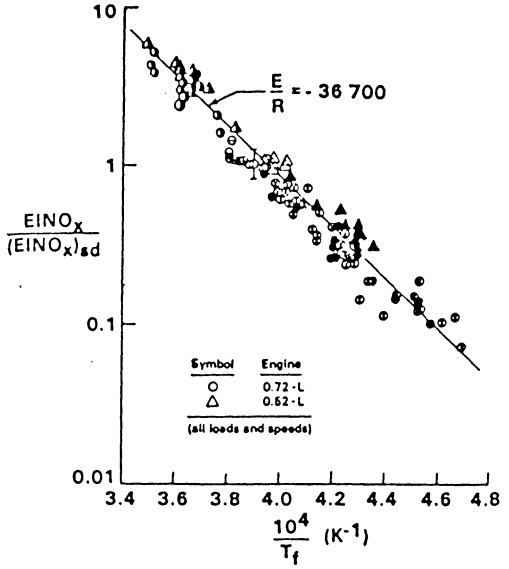

Fig. 15. Correlation of normalized $EINO_x$ with stoichiometric flame temperature for both engines, all loads/speeds.

Ahmad et al.[16] used two different temperatures instead of T_f in eq. (24). T_{f1} is the same as that used above, the other, T_{f2}, is obtained by assuming adiabatic compression of the unburned gas from the unburned gas pressure at TDC to the peak cylinder pressure. They found no significant difference between the correlations using T_{f1} and T_{f2}. Futhermore, they came to the same conclusions as Plee et al., except that E/R was slightly lower for the DI engine, as can be seen in fig. 16.

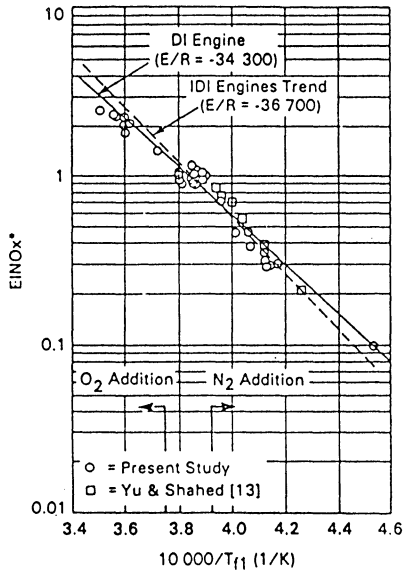

Fig. 16. Flame temperature correlations for normalized NO_x emissions from different engines.

3:2:2 EXTENDED ZELDOVICH

Wu and Peterson [18,19] have developed a model which requires measured temperature, fuel burning rate, engine speed, start of combustion and end of combustion to evaluate the NO emission index, EINO. EINO is defined as g NO/kg fuel. It is assumed that the mass of NO formed can be evaluated from

$$dm_{NO} = M_{NO}\int_0^{\tau_m} \frac{d[NO]}{dt}\, dt\, dV_b \qquad (25)$$

where $\frac{d[NO]}{dt}$ is the rate of NO formation, M is the molecular weight, τ_m is the mixing time scale, t is the time and V_b is the volume of the burned gases. During the mixing time, τ_m, turbulent mixing causes the temperature of the burned gases to decrease and the radicals involved in NO formation to recombine. Using the extended Zeldovich mechanism and assuming the reverse reactionsto be negligible and [N] to be at steady state, the rate of NO formation becomes

$$\frac{d[NO]}{dt} = 2k_{1f}[N_2][O] \qquad (26)$$

Assuming $2k_{1f}[O]dV_b \sim \exp(-E/RT)dm_f$ and the temperature to be uniform in dV_b they obtained

$$dm_{NO} \sim \int_0^{\tau_m} \exp(-E/RT)dt \; dm_f \tag{27}$$

where E, the overall activation energy, is a parameter in the model. The plausibility of assuming uniform temperature in dV_b was tested by calculating flame temperatures in extreme mixing models [20]. The calculations differed by roughly $\pm$100K which was the same as the uncertainty in the experiments performed by Wu and Peterson.

Since $dm_f = (dm_f/d\theta)d\theta$, the amount of NO formed from the mass of fuel burned, m_{fb} during combustion can be evaluated from

$$m_{NO}(m_{fb}) \sim \int_{\theta_{soc}}^{\theta} \left(\int_0^{\tau_m} \exp(-E/RT)dt\right)\frac{dm_f}{dt}\, d\theta \tag{28}$$

where θ is the crank angle and soc refers to start of combustion. The inner integral accounts for the turbulent mixing process and the outer for the coupling between the temperature history and the fuel burning rate. If both sides of eq. (28) are divided by the total mass of fuel injected, m_f, and the outer integral is evaluated over the entire combustion process, then eq. (28) becomes

$$EINO \sim \int_{\theta_{soc}}^{\theta_{eoc}} \left(\int_0^{\tau_m} \exp(-E/RT)dt\right)\frac{dF_f}{d\theta}\, d\theta \tag{29}$$

where EINO is the emission index of NO defined as the ratio of the mass of NO to the total mass of fuel injected into the combustion chamber, $\frac{dF_f}{d\theta}$ is the specific fuel burning rate and the subscript eoc refers to end of combustion.

Wu and Peterson chose two different time scales to characterize the mixing time τ_m. The first and shortest, the Kolmogorov time scale τ_k [21] can be expressed as

$$\tau_k \sim \left(\frac{N^*}{N}\right)^{3/2} \tag{30}$$

The other, the Corrsin time scale, can be expressed as

$$\tau_c \sim \frac{N^*}{N} \tag{31}$$

where N is the engine speed and N^* is a reference engine speed. Substituting (30) and (31) into (29) they obtained

$$EINO \sim \left(\frac{N^*}{N}\right)^{3/2} \int_{\theta_{soc}}^{\theta_{eoc}} \exp\left(-E/RT\right) \frac{dF_f}{d\theta}\, d\theta \tag{32}$$

$$EINO \sim \frac{N^*}{N} \int_{\theta_{soc}}^{\theta_{eoc}} \exp\left(-E/RT\right) \frac{dF_f}{d\theta}\, d\theta \tag{33}$$

If the temperature is assumed to be constant during combustion then eq. (32) and (33) reduce to

$$EINO \sim \left(\frac{N^*}{N}\right)^{3/2} \exp(-E/RT^*) \tag{34}$$

$$EINO \sim \frac{N^*}{N} \exp(-E/RT^*) \tag{35}$$

where T^* is the characteristic temperature.

The engine used in the experiment was a single–cylinder, automotive type, divided chamber with a displacement of 0.72 L and a compression ratio of 19.3. The prechamber had a cylindrical geometry. The engine conditions are shown in table 5. Figs 17, 18 and 19 show measured EINO versus the variable temperature correlation parameter; in figs 17 and 18 with E/R = 20000 K and in fig. 19 with E/R = 38000 K. The fact that the correlation with E/R =20000 K is better than the correlation with E/R = 38000 K, (38000 K is the activation temperature of reaction (1)), can be explained by the superequilibrium radical concentrations. Fig. 20 shows EINO predicted using the constant temperature correlation with a temperature calculated from the cylinder pressure at 8°CA after the end of injection versus measured EINO. Fig. 21 shows that regarding the normalized mass, the variable temperature correlation is far better. Even if no significant difference is seen between the correlations in figs 17 and 18, the Kolmogorov time scale is believed to be more plausible.

Table 5. Engine conditions.

Series	Speed (r/min)	Overall air-fuel ratio	Combustion timing (°CA)	Intake pressure (kPa)	Intake-air temperature (K)	EINO (g/kg)
1	1000	40:1	355	135	303	35.5
2*	1000	40:1	363	135	303	30.9
3	1000	40:1	367	135	303	24.4
4	1000	25:1	363	135	303	21.1
5	1000	32:1	363	135	303	28.0
6	1000	55:1	362	135	303	33.4
7	1500	40:1	363	135	303	20.6
8	2000	40:1	363	135	303	17.4
9	1000	40:1	363	100	303	29.3
10	1000	40:1	363	150	303	31.6
11	1000	40:1	362	135	325	32.4
12	1000	40:1	363	135	351	32.5

* baseline condition

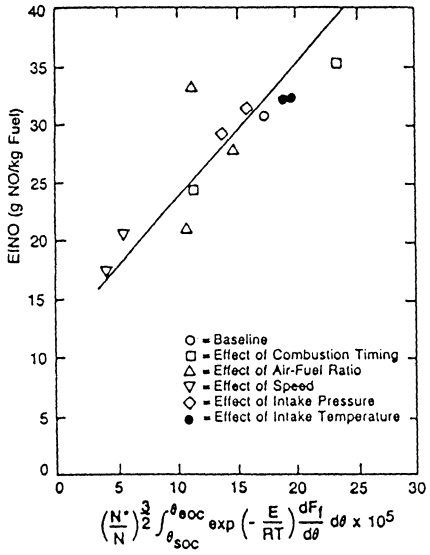

Fig. 17. Correlation of EINO with the variable–temperature correlation parameter assuming a short mixing time scale with E/R = 20000 K. The straight line represents the least–squares fit to the data.

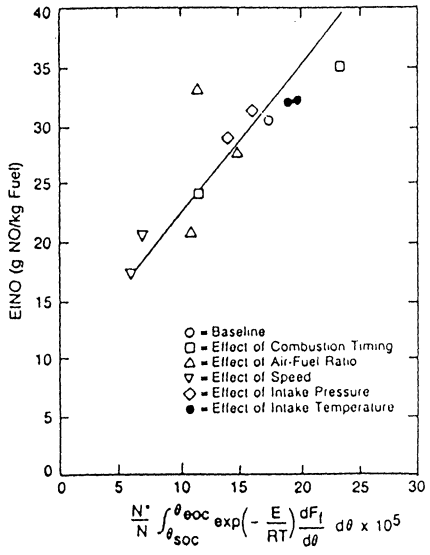

Fig. 18. Correlation of EINO with the variable–temperature correlation parameter assuming a long mixing time scale with E/R = 20000 K. The straight line represents the least–squares fit to the data.

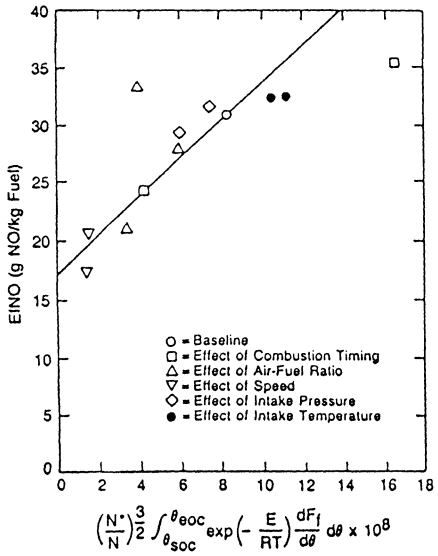

Fig. 19. Correlation of EINO with the variable–temperature correlation parameter assuming a short mixing time scale with E/R=38000K. The straight line represents the least–squares fit to the data.

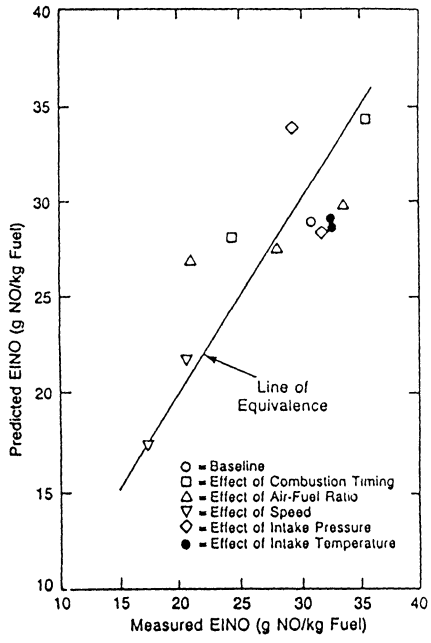

Fig. 20. Correlation of EINO with the constant–temperature correlation parameter assuming a short mixing time scale with E/R = 38000 K. The straight line represents the least–squares fit to the data.

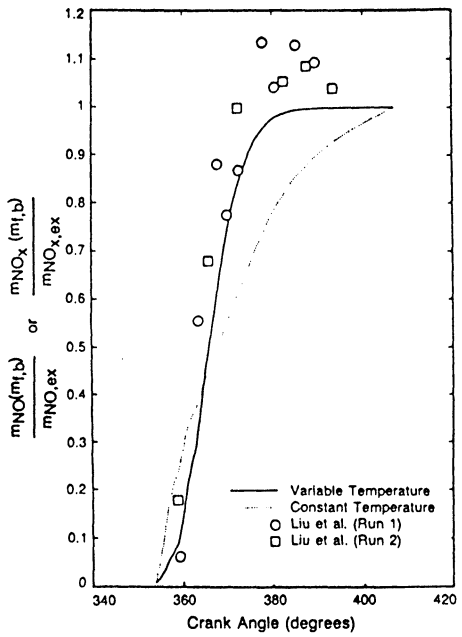

Fig. 21. Comparisions of the histories of NO formation from the variable– and constant–temperature correlations assuming a short mixing time scale and E/R = 38000 K with measured data. The engine conditions are : 1000 r/min, 40:1 overall air–fuel ratio, 355°CA combustion timing and 135 kPa intake manifold pressure.

3:3 PARTIALLY STIRRED REACTORS

The partially stirred reactor models are divided into four groups:

burned unburned zone models
spatial variations
phenomenological models
multidimensional models.

3:3:1 BURNED UNBURNED ZONE MODELS

In a burned unburned zone model the combustion chamber is divided into two zones, one in which the fuel is burned and one in which it is unburned. Cakir [22] has developed such a model. He treated the gases as perfect with variable specific heats and assumed thermodynamic equilibrium properties and composition for the burnt gas. Heat transfer to cylinder walls and heat flux between adjacent gas elements are neglected. Cakir uses the Zeldovich mechanism and by assuming [N] and [O] at steady state he obtains the NO formation rate as

$$V\frac{d[NO]}{dt} = 2(k_1/k_2)^{1/2}\left(\frac{k_{1f}[N_2][O_2]^{1/2}}{1+(k_{1b}/k_{2f})[NO]/[O_2]}\right)\left(1-\frac{k_{2b}k_{1b}[NO]^2}{k_{1f}k_{2f}[N_2][O_2]}\right)$$

The concentrations are calculated from

$$[N_2]_{ui} = [N_2]_0(1-(Z_a)_i)$$
$$[N_2]_{bi} = [N_2]_0(Z_a)_i$$
$$[O_2]_{ui} = [O_2](1-(Z_a)_i)$$
$$[O_2]_{bi} = [O_2]_0(1-(Z_s)_i/\lambda_0)(Z_a)_i$$

and the constants are given in table 6.

Table 6. Rate constants used.

Reaction	Symbol	Rate constant, cm³/mol s T, K, R = 1·986 cal/K
$O_2 \rightarrow 2O$	k_1	$6\times10^{13}\frac{118\,000}{RT}\exp\left(-\frac{118\,000}{RT}\right)$
$2O \rightarrow O_2$	k_2	$1{\cdot}0\times10^{14}$
$N_2+O \rightarrow NO+N$	k_{1f}	$7\times10^{13}\exp\left(-\frac{75\,500}{RT}\right)$
$NO+N \rightarrow N_2+O$	k_{1b}	$1{\cdot}55\times10^{13}$
$N+O_2 \rightarrow NO+O$	k_{2f}	$13{\cdot}3\times10^{9}T\exp\left(-\frac{7080}{RT}\right)$
$NO+O \rightarrow N+O_2$	k_{2b}	$3{\cdot}2\times10^{9}T\exp\left(-\frac{39\,100}{RT}\right)$

The volumes of the unburned and burned zones are:

$$V_{ui} = V_0(1-Z_{ai})\left(\frac{P_0}{P_i}\right)^{1/\gamma_u}$$
$$V_{bi} = V_i - V_{gi}$$

where P_i is the cylinder pressure at time i and γ is the ratio of specific heats given by

$$C_{vg} = 4.1855(F_p+0.02\,T_b^{0.6})$$
$$C_{va} = 4.1855(4.61\,A_r + 6.5\cdot10^{-4})$$

where C_{vg} is the specific heat of burned gas, C_{va} is the specific heat of air, F_p is an initial value changing with air–fuel ratio and A_r is the recirculated exhaust gas factor which varies between 1.0 and 1.03. The temperature to be used in the rate constants is the real burnt gas temperature T_{bi}

$$T_{bi} = \frac{((Z_a)_{i-1} T_i^{''}) + ((Z_a)_i - (Z_a)_{i-1}) T_i^{'}}{(Z_a)_i} \tag{36}$$

where $(Z_a)_{i-1}$ is the fraction of air in percent at time i–1, $T_i^{''}$ represents the temperature of gases burned at time i–1 and adiabatically compressed or expanded and $T_i^{'}$ represents the temperature of the fraction of gas burned last and compressed or expanded adiabatically.

$$(Z_a)_i = (Z_a)_{i-1} + \frac{(Z_k)_i - (Z_k)_{i-1}}{Z_s} \tag{37}$$

where $(Z_k)_i$ is the fraction of heat released in percent and Z_s is the reciprocal of the mixture enrichment factor.

$$Z_s = \frac{\lambda_0 C_z}{B(\exp(T_z - Z_k)^2 \lambda_0^a)} \tag{38}$$

where C_z,B,T_z and a are constants to be determined and λ_0 is the air–fuel ratio before combustion.

$$T_i^{''} = T_{b(i-1)} \left(\frac{P_i}{P_{i-1}}\right)^{\frac{\gamma-1}{\gamma}} \tag{39}$$

where γ is the ratio of specific heats.

$$T_i^{'} = T_{u(i-1)} + \frac{Z_s Q}{MC_{vm}} \left(\frac{P_i}{P_{(i-1)}(1+Y(P_{(i-1)})^{1/\gamma-1})}\right)^{(\gamma-1)/\gamma} \tag{40}$$

where T_u is the temperature of unburned gases, Q is the heat release, M is the number of moles, $Y = Q(\gamma-1)/P_0^{1/\gamma}V_0$ and V_0 is the volume before combustion. The heat release Q is calculated from

$$\frac{dQ}{dt} = \frac{C_v}{R}\left(\gamma P \frac{dV}{dt} + V \frac{dP}{dt}\right) \tag{41}$$

using a P–t diagram.

$$C_{vm} = C_{vg} Z_{a(i-1)} + C_{va}(1 - Z_{a(i-1)}) \tag{42}$$

Cakir tried the model on a single–cylinder test engine (International Harvester) and a spark–ignited diesel hybrid (a 6–cylinder M.A.N. D1246–FM). A comparision between predicted and measured nitric oxide emissions for variable load on the International Harvester is shown in fig. 22, and for the diesel hybrid in figs 23, 24 and 25.

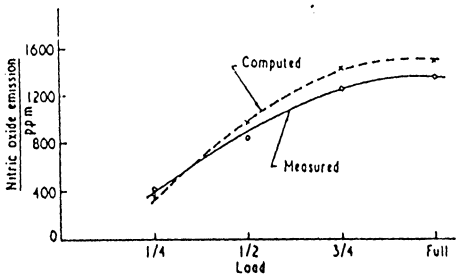

Fig. 22. Measured and predicted NO emission at variable load. International Harvester single–cylinder test engine. N = 2000 rpm, C_r=17.

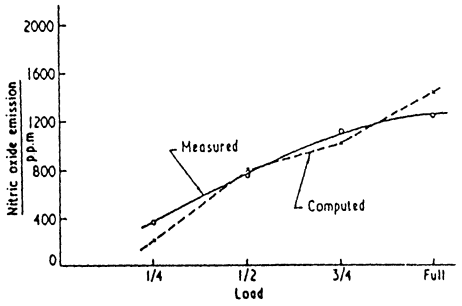

Fig. 23. Measured and predicted NO emission at variable load. Four–stroke, six–cylinder M.A.N. D1246–FM engine. N = 2000 rpm, C_r = 17.

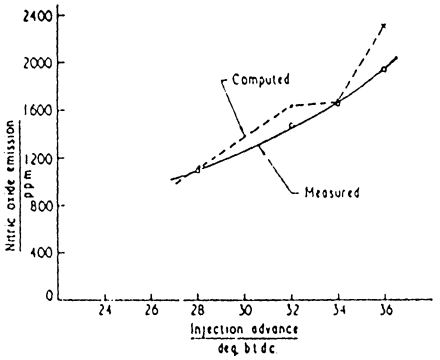

Fig. 24. Measured and predicted NO emission under variable injection advance. Four–stroke, six–cylinder M. A. N. D1246–FM engine. N = 1500 rpm, C_r = 17, 3/4 load.

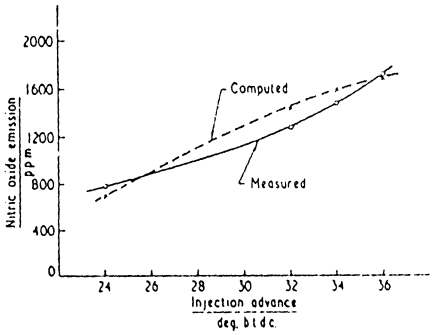

Fig. 25. Measured and predicted NO emission under variable injection advance. Four–stroke, six–cylinder M.A.N. D1246– FM engine. N = 1500 rpm, C_r = 17, full load.

The input data needed for the prediction are the volume before combustion V_0, fuel–air ratio before combustion λ_0, and a pressure–time diagram for the engine.

3:3:2 SPATIAL VARIATIONS

An attempt to model the effects of Exhaust Gas Recirculation (EGR) has been made by Ikegami et al.[23]. They used the Zeldovich mechanism to obtain

$$[NO] = \int\int \exp(-E/R\bar{T})[\bar{O}_2]^{1/2} f(t,v)dtdv \tag{43}$$

where f(t,v) describes the temporal and spatial variations. Assuming f(t,v) does not depend on the degree of EGR, the ratio of [NO] with EGR to [NO] without EGR is expressed as

$$\frac{[NO]}{[NO]_0} = ([\bar{O}_2]/[\bar{O}_2]_0)^{1/2} \frac{\exp(-E/R\bar{T})}{\exp(-E/R\bar{T}_0)} \equiv \alpha([\bar{O}_2]/[\bar{O}_2]_0)\beta(\bar{T},\bar{T}_0)$$

The factor α is a measure of the effect of oxygen concentration. The factor β is a measure of the effect of temperature. The effect of the spatially averaged temperature T_m gives β_m=1. The flame temperature gives β_f

$$\beta_f = \exp\left(\frac{-E}{RT_{f0}} \cdot \frac{\Delta T_f}{T_{f0}-\Delta T_f}\right) \tag{44}$$

where T_{f0} is the flame temperature without EGR,

$$\Delta T_f = T_{f0} - T_f = \frac{r' H_u L_0}{c(1+L_0)(1+L_0-r')} \tag{45}$$

where c is the constant specific heat of gas, H_u is the lower calorific value of the fuel, L_0 is the stoichiometric air requirement and

$$r' = \frac{Gr'}{Ga+Gr} \tag{46}$$

where Gr′ is the quantity of inert gas contained in Gr and Gr and Ga are the quantities of recycling gas and inlet air, respectively. The temperature drop due to limited oxygen supply gives β_ϕ. β_ϕ is calculated from eq. (44) by exchanging T_{f0} and ΔT_f with T_{m0} and ΔT_ϕ.

$$\Delta T_\phi = \frac{H_u}{c\phi_0^*}\left(\frac{1}{1+L_0/\phi_0^*} - \frac{1-r'}{1+(1-r')L_0/\phi_0^*}\right) \tag{47}$$

where ϕ_0^* is the local equivalence ratio without EGR. This model can only give relative values for an engine. Fig. 26 shows measured $[NO]/[NO]_0$, β_m, β_ϕ and β_f versus r′.

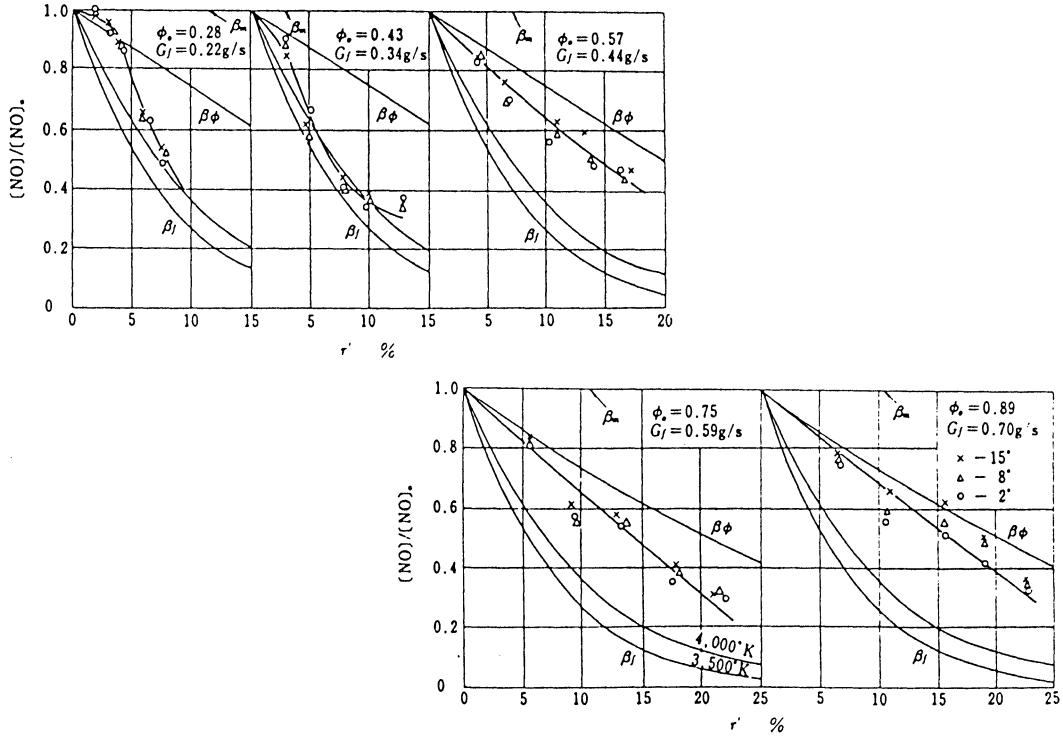

Fig. 26. $[NO]/[NO]_0$ versus net percentage of EGR r′ for the spatial variations model.

3:3:3 PHENOMENOLOGICAL MODELS

Phenomenological models are based upon some conceptualization of each individual process occurring in the engine cycle [24]. The processes are

fuel injection
fuel evaporation and ignition delay
heat release rate and heat losses
exhaust emissions.

In fig. 27 a schematic diagram of the diesel combustion process is shown. The fuel is injected through a nozzle and forms a spray with characteristic parameters as shown in fig. 28. Many expressions for the spray angle θ, the Sauter Mean Diameter (SMD), the breakup length and the spray tip penetration have been developed [24,25]. The pre–ignition processes are both physical and chemical. The evaporation rate controls the physical delay. In the physical delay period the fuel is atomized, vaporized, mixed with air and raised in temperature. The phenomenological models are divided into single zone, two– to four–zone and multizone models.

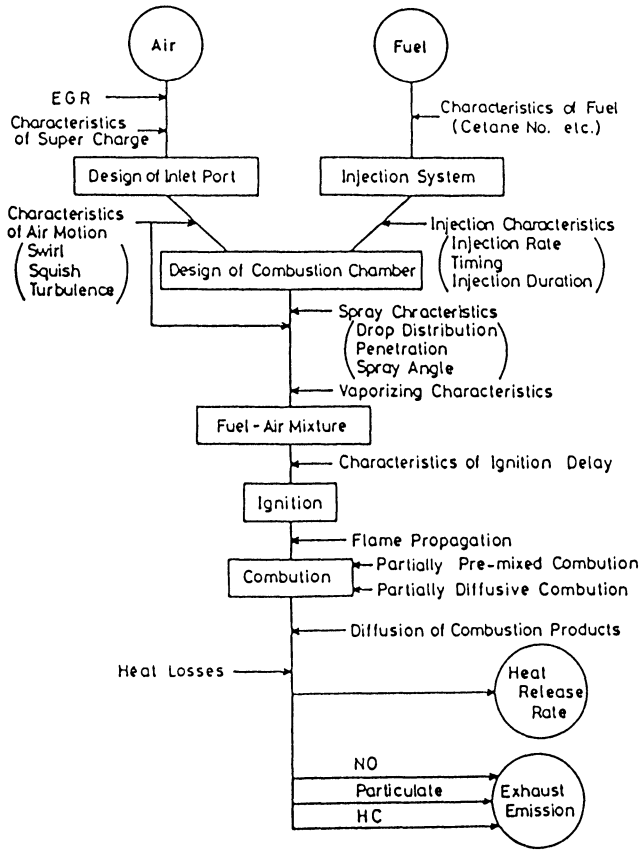

Fig 27. Block diagram illustrating diesel combustion.

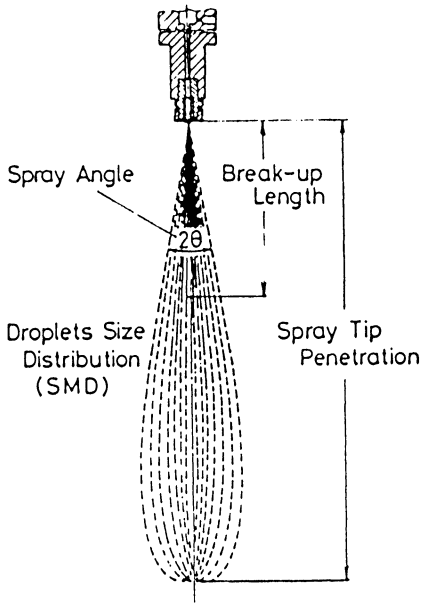

Fig. 28. Parameters used to define a spray.

SINGLE ZONE MODELS

Dent et al. [38][39][40] have developed a single–zone phenomenological model. They used characteristic mixing rates based on the dissipation of turbulent kinetic energy in the engine cylinder after injection to model the mixing of air and fuel. No allowance was made for fuel impingement on the wall. The NO formation rate used was obtained from the Zeldovich mechanism and is given by

$$\frac{1}{V_{bv}}\frac{d}{dt}([NO]V_{bv}) = 2(1-\alpha^2)\frac{R_1}{1+\alpha R_1/R_2} \tag{48}$$

$$\alpha = \frac{[NO]}{[NO]_{eq}}$$

$$R_1 = k_1[N]_{eq}[NO]_{eq}$$

$$R_2 = k_2[N]_{eq}[O_2]_{eq}$$

where V_{bv} is the volume of burning mass. The equilibrium concentrations are calculated from the equilibrium constants of reactions (1) and (2) and O_2 dissociation, mass balance equations and the ideal gas law. The data required for the prediction are:

the engine dimensions
operating conditions
fuel injection pressure diagram and
swirl ratio at inlet valve closure

They used the injection pressure diagram synthesized by line segments and discretized elements to calculate the injected fuel quantity, spray penetration, Sauter mean diameter of atomized droplets, fuel droplet size distribution and air entrainment into the spray over the discretized time step Δt. The injected fuel quantity $\dot{Q}$ is calculated from

$$\dot{Q} = C_d(2\Delta P/\rho_f)^{1/2}A_0 \tag{49}$$

where C_d is the orifice discharge coefficient, ρ_f the fuel density, ΔP is the difference between the fuel line and the engine pressures over Δt and A_0 is the nozzle orifice area.

In a quiescent chamber spray penetration is evaluated from

$$S = 0.39(2\Delta P/\rho_f)^{1/2}t \tag{50}$$

when $t < 0.3$ ms, otherwise from

$$S = (8U_0d_0't)^{1/2}(294.4/T)^{1/4} \tag{51}$$

where t is the time from start of injection, U_0 is fuel jet velocity and d_0' is the equivalent jet orifice diameter,

$$U_0 = (2\Delta P/\rho_f)^{1/2} \tag{52}$$

$$d_0' = d_0(\rho_f/\rho_a)^{1/2} \tag{53}$$

d_0 is the orifice diameter.

The SMD is calculated from

$$SMD = 8.0\ \Delta P^{-0.458}\ Q^{0.209}\ \nu_f^{0.215} \tag{54}$$

where ν_f is the kinematic viscosity of the fuel. The radial droplet size distribution is schematically shown in fig. 29. Y_P is the normalized radius Y/r_j, r_j is the jet radius, $D_P = d_P/SMD$ and d_P = droplet diameter.

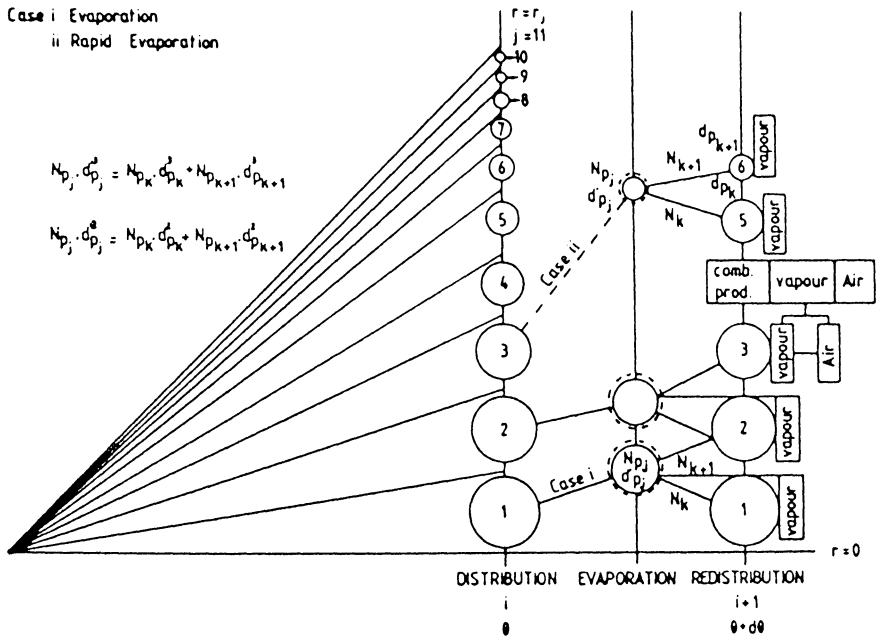

Fig. 29. Schematic of droplet distribution, evaporation and burning mechanisms.

The jet structure is given by

$$dr_j/dS = 0.11(\rho_a + \rho_j)/\rho_j \tag{55}$$

$$U/U_m = (1-Y_P^{3/2})^2 \tag{56}$$

$$f/f_m = (U/U_m)^{1/2} \tag{57}$$

where ρ_a is the density of air, U is the local velocity at Y_P, U_m is the jet centre–line velocity at S, and f is the mass concentration at S on the jet centre–line. The air entrainment is obtained from

$$(\dot{m}_{aE} + \dot{m}_f)/\dot{m}_f = 0.32\ S/d_0 \tag{58}$$

where $\dot{m}_{aE}$ and $\dot{m}_f$ are mass flow rates of air entrained and fuel injected, respectively. Air entrainment into a wall jet is calculated from

$$(\dot{m}_{aw} + \dot{m}_f)/\dot{m}_f = 0.865\ S_w/d_0' \tag{59}$$

where S_w is the wall jet penetration in time Δt, and the origin of S_w is the intersection of the jet axis and the impingement surface. At the end of the injection period, the turbulent mixing contributes to the air entrainment. The mass of air entrained, dm_a/dt, is obtained from

$$dm_a/dt = C_1(m_a/\tau) \tag{60}$$

where C_1 is a constant and τ is the mixing time.

$$\tau = (L^2/\epsilon)^{1/3} \tag{61}$$

where L is the length scale , here taken as d_0', and ϵ is the energy dissipation rate of the eddy structure.

$$\epsilon = C\ (N/\theta_{ip})^3(V_f/nd_0^{\ 2})^2 \tag{62}$$

where C is a known constant [53], N is the engine speed, θ_{ip} is the injection period, V_f is the volumetric delivery of fuel per stroke of the injection pump, n the number of holes in the injector nozzle and d_0 the injector orifice diameter. When swirl is added to the engine the air entrainment and jet structure are affected. The turbulent mixing is given by

$$R = R_{inj}R_{swirl}/(R_{inj} + R_{swirl}) \tag{63}$$
$$R = 1/\tau$$

PHYSICAL PROCESS	MODEL	
	QUIESCENT CHAMBER	SWIRL CHAMBER
Fuel volumetric injection rate	$\dot{Q} = C_d (2\Delta P/\rho_f)^{\frac{1}{2}} A_o$	
Fuel jet velocity	$U_o = (2\Delta P/\rho_f)^{\frac{1}{2}}$	
Fuel spray penetration	$t < 0.3$ ms $S = 0.39 (2\Delta P/\rho_f)^{\frac{1}{2}} t$ $t > 0.3$ ms $S = (8 U_o d_o' t)^{\frac{1}{2}} (294.4/T)^{\frac{1}{4}}$	$\frac{S-S_w}{S} = 0.35 (\frac{S_w J_a}{d_o' J_f})^{\cdots}$
Rate of jet growth	$dr_j/dS = 0.11(\rho_a+\rho_j)/\rho_j$	$dr_j/dS = 0.11(U_m/U_m+U_T)$ $(\frac{\rho_j}{\rho_a+\rho_j})$
Radial distribution of velocity profile	$\frac{U}{U_m} = (1 - Y_p^{3/2})^2$	
Mass concentration profile	$f/f_m = (U/U_m)^{\frac{1}{2}}$	
Free jet air entrainment	$(\dot{m}_{ae}+\dot{m}_f)/\dot{m}_f = 0.32 \times S/d_o'$	$d\dot{m}_{ae}/dS = 2\pi r_j (\rho_m \rho_a)^{\frac{1}{2}}$ $(a_1\lvert U_m - U_t \rvert) + a_2 \lvert U_n \rvert)$
Fuel jet temperature profile	$(T-T_a)/(T_f-T_a) = f$	
Sauter Mean Diameter	$SMD = 8.0\ \Delta P^{-0.454} \dot{Q}^{0.289}\ \nu_f^{0.215}$	
Cumulative volume fraction	$0.082 < D_p < 3$ $V_{cf} = \exp(0.05328 D_p - 0.54174\ D_p^2)$	
Radial fuel droplet size distribution	$-dD_p/dY_p = (1/V_{fl})(dV_{fl_{Y_p}}/dY_p)/$ (dV_{cf}/dD_p)	
Wall jet penetration	$S_w = (2.06 U_j d_o' t_w)^{\frac{1}{2}}$	
Wall jet air entrainment rate	$\dot{m}_{aw}+\dot{m}_f/\dot{m}_f = 0.866\ S_w/d_o'$	

Air entrainment after the end of injection		$m_a/m_{aa} = \exp(-C_1 t/\tau)$	
COMBUSTION MECHANISM		LEAN REGION $\phi > 1$	RICH REGION $\phi > 1$
	Mass of fuel burnt	Total fuel mass available	Stoichiometric fuel-vapour-air ratio times the mass of air available
	Mass of air consumed	Stoichiometric air-fuel ratio times the mass of fuel available	Total mass of air available
Amount of heat release due to combustion		$d\dot{Q}_{ret} = d\dot{m}_{vb} H_o$	
Heat transfer from cylinder gass to the wall		$\dot{Q}_{tr} = h_j A_c (T_{ch} - T_w)$	
Air swirl		Not required	$\omega_c = \frac{(\frac{D}{2})^2}{n(\frac{D}{2})^2 \frac{L(0)}{V_{bo}} + (\frac{d}{2})^2} \omega_o$ $\frac{n(\frac{D}{2})^2 \frac{L(0)}{V_{bo}} + 1}{}$ $U = \omega . r$ (solid body rotation, forced vortex flow)
Spray deflection		Not required	$\frac{dI}{dS} = \frac{2 U_t E_t}{V_j U_m^2 R}$ $+ \frac{C_d U_n \lvert U_n \rvert}{\pi r_j U_m^2 R}$

Fig. 30 Brief description of the single–zone model.

Table 7. Test conditions for quiescent chamber–single cylinder four–stroke direct–injection diesel engine.

ENGINE 1

Test Condition \ Data Set	A	B	C	D	E
Engine speed (rpm)	1300	1900	1300	1300	1300
Injection timing (BTDC)	18	10	10	24	16
Injection duration (°CA)	24	28	24	30	30
Fuelling rate (mm^3/cycle)	142.3	142.3	142.3	191.6	191.6
Intake pressure (bars)	1.19	1.35	1.19	1.5	1.5
Intake temperature (°K)	333	333	333	333	333

Bore = 140 mm, Stroke = 152.4 mm
Compression ratio = 14.3
Number of nozzle holes = 8
Orifice diameter = 0.2032 mm
Air /fuel ratio = 25
l_o/d_o = 4

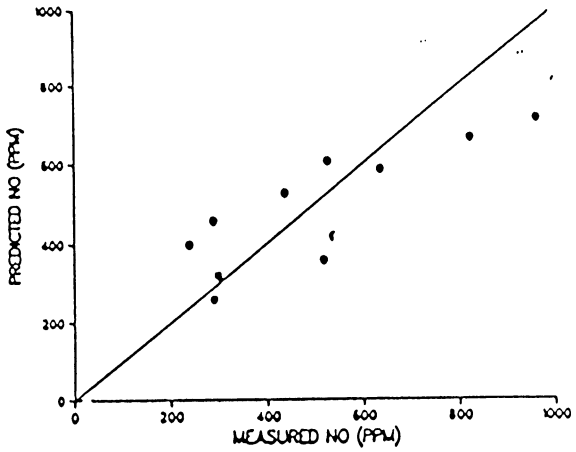

Fig. 31. Quiescent NO model overall comparison with engine data (see table 9).

The model is described in fig. 30. The model has been tried on two engines [39], tables 7 and 8. Fig. 31 and table 9 show a comparision between predicted and measured NO for engine 1. In figs 32 and 33 predicted and measured smoke–NO–EGR trade–offs are shown for engine 1, and in figs 34 and 35 predicted and measured smoke–NO–injection timing trade–offs are shown for engine 3. The model also predicts the amount of soot formation.

Table 8. Test conditions for quiescent chamber single–cylinder four–stroke direct–injection diesel engine.

ENGINE 3

Test Condition \ Data Set	COMPRESSION RATIO 18.4:1			COMPRESSION RATIO 20.4:1		
Engine speed (rpm)	1900	1900	1900	1900	1900	1900
Injection timing (BTDC)	9	12	15	9	12	15
Injection duration (°CA)	30	30	30	30	30	30
Fuelling rate (mm^3/cycle)	121.9	119.1	115.9	121.9	117.8	114.9
Intake pressure (bars)	2.27	2.21	2.16	2.31	2.24	2.19
Intake temperature (°K)	315	316	317	312	315	315

Bore = 120 mm, Stroke = 120 mm
Number of nozzle holes = 7
Air/fuel ratio = 28
Orifice diameter = 0.17 mm
l_o/d_o = 7

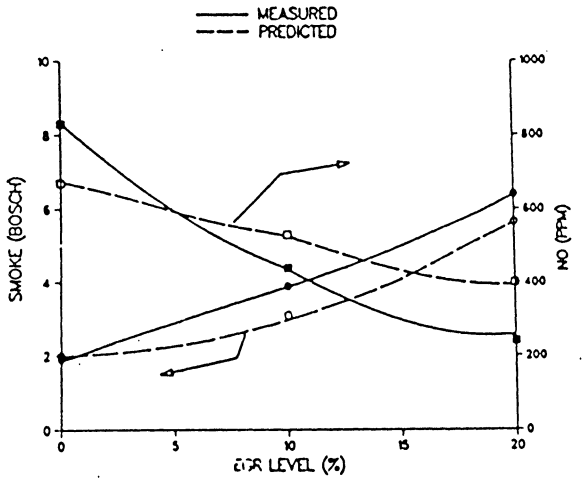

Fig. 32. Smoke–NO–EGR trade–off set E table 7.

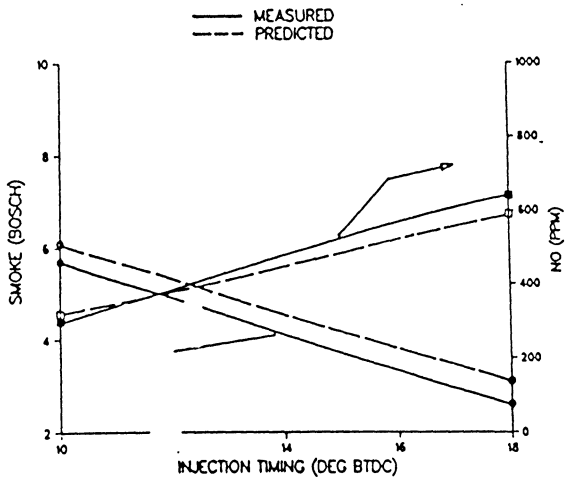

Fig. 33. Smoke–NO–trade–off sets A and C table 7.

Table 9. Comparision between predicted and experimental nitric oxide concentrations. Single–zone model.

SET A	EXP (PPM)	PRED (PPM)
10 EGR	640	590
20 EGR	290	460
SET B		
0 EGR	520	360
10 EGR	290	260
SET C		
0 EGR	540	420
10 EGR	300	320
SET D		
10 EGR	970	720
20 EGR	530	610
SET E		
0 EGR	830	670
10 EGR	440	530
20 EGR	240	400

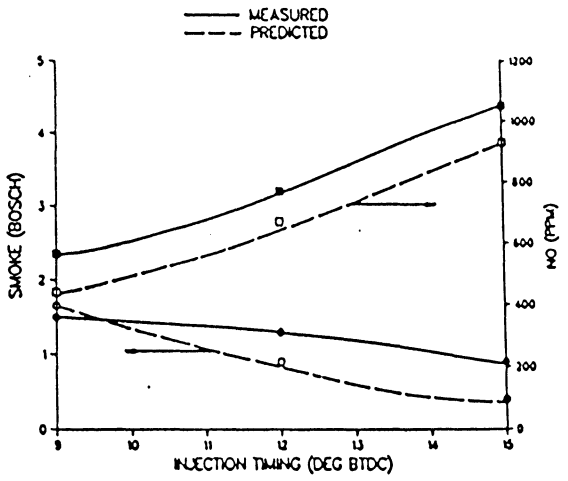

Fig. 34. Smoke–NO–injection timing trade–off, compression ratio 18.4:1,table 8.

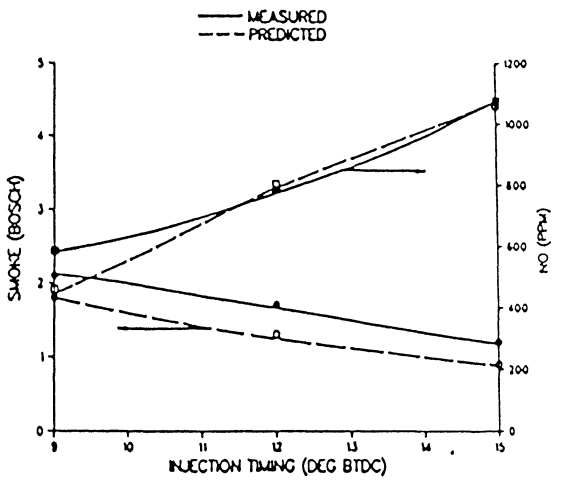

Fig. 35. Smoke–NO–injection timing, trade–off, compression ratio 20.4:1, table 8.

MULTIZONE MODELS – NO MIXING

Hiroyasu et al.[29] have developed a model which is divided into a Heat Release (HR) and an Emission Formation (EF) model. In the HR model, fuel injected through the nozzle is divided into 250 packages with the same fuel mass. It is assumed that there is no mixing between the packages. Spray impinging on walls and swirl are considered. The air entrainment into the spray is given by the conservation of momentum and the spray behaviour is determined by the experimental equation of spray penetration observed without combustion. In fig. 36 a schematic diagram of spray combustion is presented and fig. 37 shows the combustion process of each package. Droplet evaporation, which is assumed to start immediately after injection, is modelled. The heat release rate is calculated in each package, and by summing up the heat release from each package, the heat release in the combustion chamber is obtained, from which it is possible to calculate the average temperature and the pressure. Heat transfer to the walls is accounted for.

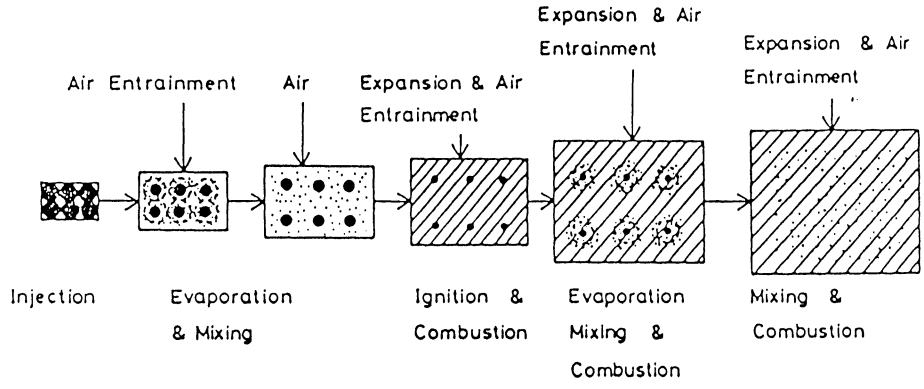

Fig. 36. Schematic diagram of the spray combustion in the "no mixing" model.

NO forms via the extended Zeldovich mechanism. A heterogeneous temperature field is assumed. The adiabatic flame temperature $T_B(\theta_a)$ is calculated as in homogeneous combustion. After combustion the adiabatic temperature varies as

$$T_B(\theta) = T_B(\theta_a)\,(P(\theta)/P(\theta_a))^{\frac{\kappa-1}{\kappa}} \tag{64}$$

in each package.

The NO formation rate is given by

$$\frac{dY}{d\theta}NO = \frac{2R_1(1-\beta^2)}{\beta R_1/(R_2+R_3)+1}\,\frac{RT_B}{P}\,\frac{1}{\omega} \tag{65}$$

$$\beta = \frac{[NO]}{[NO]_e}$$

$$R_1 = k_{1b}[NO]_e[N]_e$$
$$R_2 = k_{2f}[N]_e[O_2]_e$$
$$R_3 = k_{3f}[N]_e[OH]_e$$

$\frac{dY}{d\theta}NO$ is the increase in mole fraction per unit crank angle. The species concentrations are calculated from the heat release model. Eq. (65) is integrated for each package from the start of burning to a crank angle where reaction rates are so low that Y_{NO} no longer changes. Finally, Y_{NO} is summed up over all the packages.

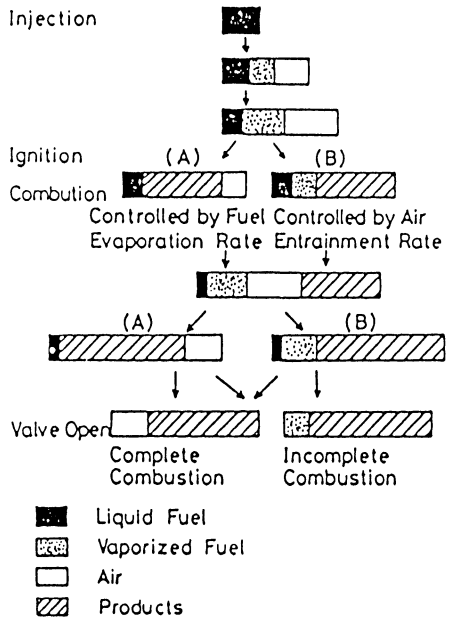

Fig. 37. Schematic diagram of the mass system in a package.

Hiroyasu et al. [30] extended the model to include additional control volume for a swirl chamber so that an IDI diesel engine could be modelled. Soot formation is also modelled. In figs 38, 39 and 40 comparisions between calculated and experimental NO and soot formations for a DI engine are shown, and in fig. 41 a comparision is presented between measured and predicted pressure for an IDI engine. Hiroyasu et al. [31] have also used this model and the "method of system – model transformation" to optimize a DI diesel engine. The parameters optimized were :

number of nozzle holes
diameter of nozzle hole
diameter of Toroidal
swirl ratio
clearance volume
intake valve closing timing
injection timing
injection duration
exhaust valve opening timing.

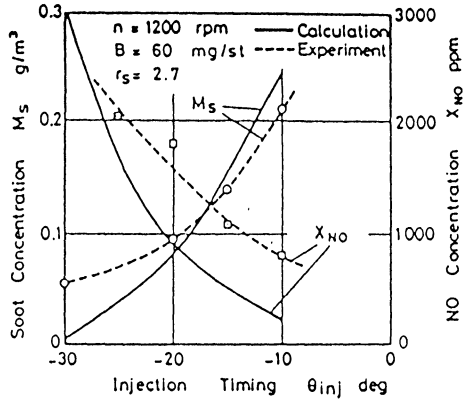

Fig. 38. Effect of injection timing on calculated and experimental soot and NO concentrations.

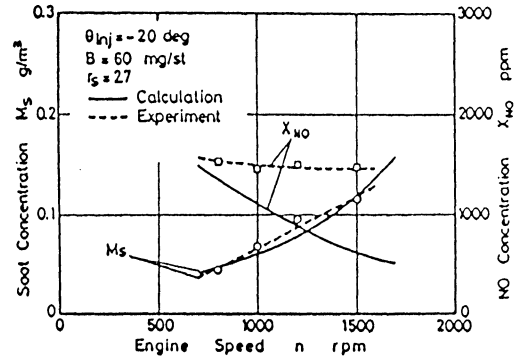

Fig. 39. Effect of engine speed on calculated and experimental soot and NO concentrations.

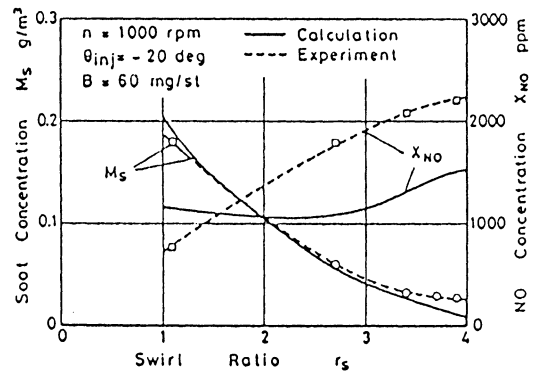

Fig. 40. Effect of swirl ratio on calculated and experimental soot and NO concentrations.

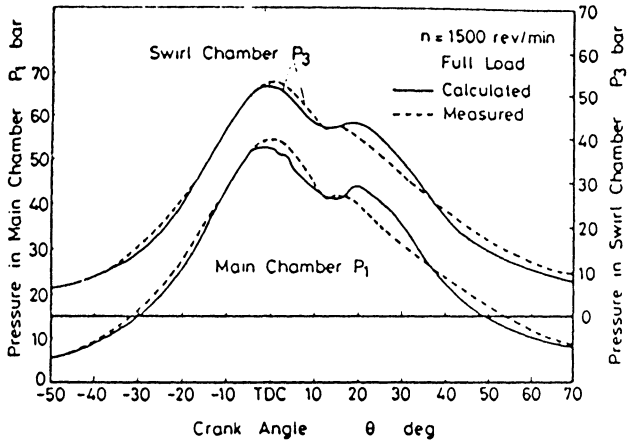

Fig. 41. Comparision between the computed and measured pressure.

STOICHASTIC MIXING

Mansouri et al. [33][34] have developed a model for an IDI diesel engine. The combustion chamber is divided into three zones, the prechamber, the main chamber and the connecting passageway. Each zone contains a large number of equal mass elements. The cycle simulation is divided into four processes, intake, compression, combustion and expansion and exhaust processes.

The intake process starts at the time the intake valve opens, t_{ivo}. Values for temperature, pressure and fuel–air equivalence ratio are assumed and checked with values obtained at the end of the cycle simulation. Quasi–steady one–dimensional flow equations are used to model the intake process. Mass flows through valves are computed using the equations for isentropic adiabatic flow through a nozzle,

$$m' = C_d A p_0/RT_0 (\gamma RT_0)^{1/2}(\frac{2}{\gamma-1}((\frac{p_s}{p_0})^{2/\gamma}-(\frac{p_s}{p_0})^{(\gamma+1)/\gamma}))^{1/2}$$

where m' is the mass flow rate through a restriction, C_d is the discharge coefficient, A is the area of the restriction, p_0 is the stagnation pressure upstream of the restriction, R is the gas constant, γ is the ratio of specific heats and p_s is the static pressure at the restriction. The mass in each chamber at t_{ivo} is obtained from

$$pV = mRT \tag{66}$$

and the the mass is calculated using

$$m' = m'_i - m'_e \tag{67}$$

where m' is the mass change in chamber, m'_i is the mass flow rate into the chamber and m'_e that out of the chamber. The rate of change of pressure, p', is obtained from

$$p_p' = p_p(T_p'/T_p + m'_{mp}/m_p) \tag{68}$$

$$p_m' = p_m(\frac{T_m'}{T_m}\frac{V_m'}{V_m} + \frac{m'_{im} - m'_{mp}}{m_m}) \tag{69}$$

where the subscripts i, m and p denote intake valve, main and prechamber, so m'_{im} denotes mass flow from intake manifold into the main chamber. T', the time rate of change of temperature is obtained from

$$T' = \frac{RT}{C_p - R}(\frac{Q'}{mRT} + \frac{m'_i(h_i - h)}{mRT} + \frac{m'_i - m'_e}{m} - \frac{V'}{V}) \tag{70}$$

where R is the average gas constant for the chamber contents, C_p is the specific heat at constant pressure, Q' is the rate of heat transfer to the chamber contents, m is the mass in the chamber, h_i is the specific enthalpy of material flowing into the chamber, h is the average specific enthalpy of the chamber contents and V' is the rate of change of volume V of the chamber.

The compression process starts at the time the intake valve closes, t_{ivc}, and is defined as part of the intake process, except that there is no flow through the intake valve.

The combustion and expansion process starts at the time the fuel injection starts t_{fis}. The fuel injection profile $m'_{fi}(t)$ is used as input. The mass of fuel injected is given by

$$m_{fi}(t) = \int_{t_{fi\,s}}^{t} \dot{m}_{fi}(t)dt \tag{71}$$

Fuel evaporation is modelled as

$$\frac{dm_{fe}}{dt} = \frac{m_{fi} - m_e}{\tau_e(t)} \tag{72}$$

where dm_{fe}/dt is the rate of evaporation of liquid fuel in the spray, m_{fe} is the mass of fuel evaporated and $\tau_e(t)$ is the characteristic evaporation time. The chemical ignition delay time τ_{id} is calculated from

$$\tau_{id}(t) = 2.43 \cdot 10^{-9}\, p^{-2} \exp(41560/RT) \tag{73}$$

Fuel–air mixture elements whose residence times and ignition delay times satisfy

$$\int \frac{dt}{\tau_{id}(t)} \geq 1$$

and whose equivalence ratio ϕ satisfy

$$\phi_L \leq \phi \leq \phi_U$$

where ϕ_L is the lower limit and ϕ_U the upper, are assumed to become burned elements instantaneously. ϕ_L and ϕ_U are inputs to the model. The work transfer to the piston is calculated from the pressure and the rate of change of volume in the main chamber. The pressure and temperature are calculated with the aid of the heat transfer to the walls, and mass and energy continuity equations. Turbulent flow Nusselt–number Reynolds–number correlations determine the heat transfer. Elements that flow into the main chamber mix with elements in it at a rate governed by the stochastic mixing model.

The exhaust process starts at the time the exhaust valve opens, t_{evo}, and is modelled as the intake process. The extended Zeldovich mechanism gives the NO formation rate

$$\frac{d(NO)}{dt} = \frac{2M_{NO}R_1(1-\alpha^2)}{\rho(1+\alpha K_1)} \tag{74}$$

where (NO) is the mass fraction, M_{NO} is the molecular weight of NO, $R_1 = k_{1f}[N_2]_e[O]_e$, $[\,]_e$ is the equilibrium mole fraction, $\alpha = [NO]/[NO]_e$, ρ is the gas density and

$$K_1 = \frac{k_{1f}[N_2]_e[O]_e}{k_{2f}[N]_e[O_2]_e + k_{3f}[N]_e[OH]_e}$$

Table 10. Cycle simulation input parameters.

I. Geometrical and Design Parameters

1. Bore
2. Stroke
3. Connecting rod length
4. Pre-chamber volume
5. Main-chamber volume
6. Passageway diameter
7. Intake valve diameter
8. Exhaust valve diameter
9. Intake valve opening time
10. Intake valve closing time
11. Exhaust valve opening time
12. Exhaust valve closing time

II. Operating Parameters

1. Intake manifold pressure
2. Inlet mixture Temperature
3. Exhaust system pressure
4. EGR rate in intake
5. Load: mass of fuel injected per cycle
6. Speed
7. Injection timing
8. Pre-chamber wall temperature
9. Main-chamber wall temperature
10. Passageway wall temperature

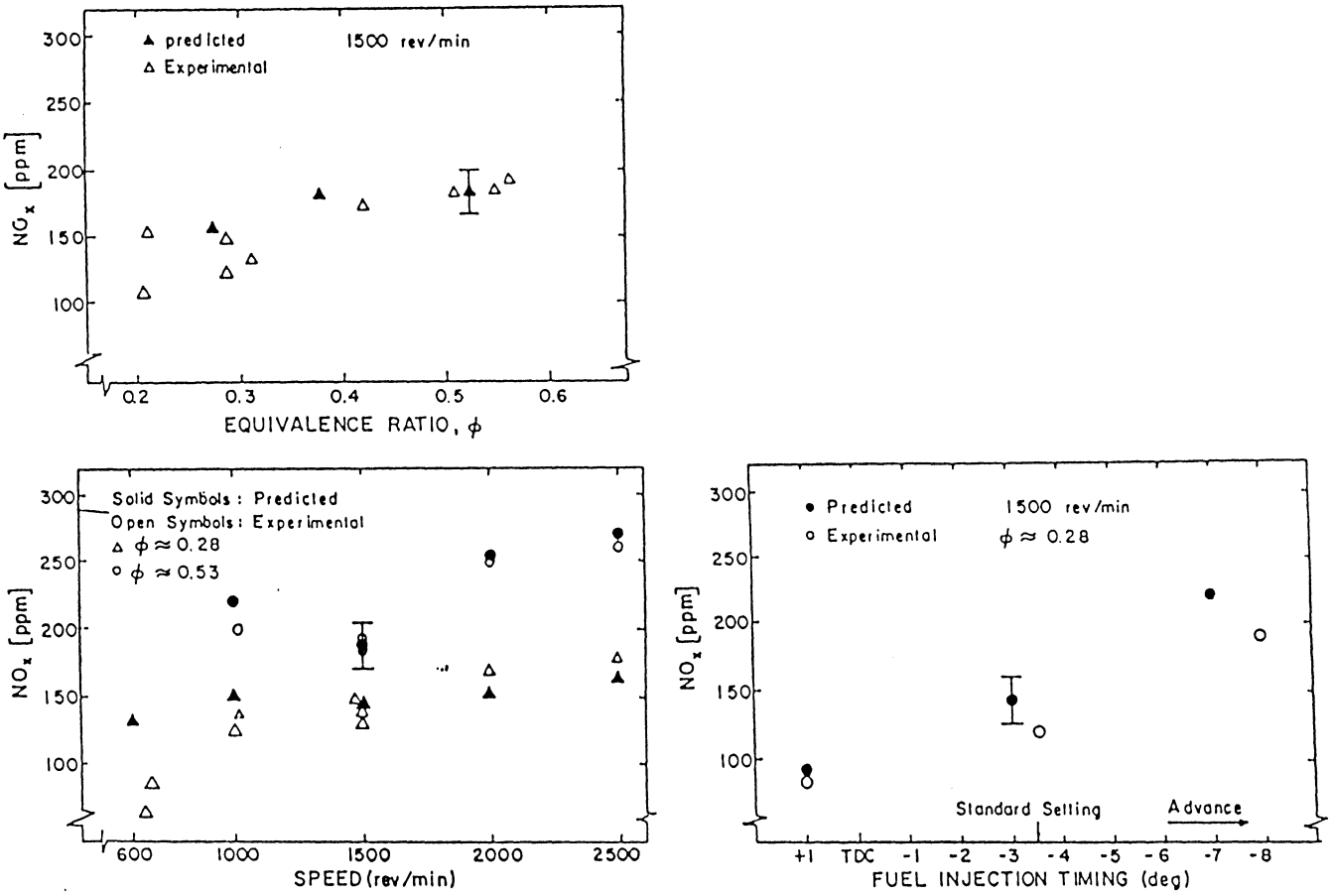

Fig. 42. Comparison of predicted exhaust NO concentrations and measured exhaust concentrations as a function of fuel–air equivalence ratio, engine speed and fuel injection timing.

The equilibrium species concentrations are calculated using a NASA equilibrium program. In fig. 42 a comparision between predicted and measured NO_x concentrations is presented. The concentration is defined as mass in chamber·[NO] in chamber/total mass in cylinder. The NO exhaust is obtained by following the NO formation in each package from the start of combustion to the start of exhaust and then summing. Soot formation is also modelled. In table 10 the input data required are listed.

The model includes eight constants that are determined from the best fit to experimental data. The constants are the passageway discharge coefficient, C_{dpw}, the mean liquid droplet size, d, the upper limit of combustion, ϕ_U and five constants in the heat transfer and turbulent mixing submodels. Variation of these constants one at a time showed $[NO_x]$ to be slightly dependent on them.

Liu et al. [35] used the model to examine the effects of fuel injection timing and EGR on a single–cylinder version of a 1979 Oldsmobile diesel engine with naturally aspirated four–stroke indirect injection. The solid line in figs 43, 44 and 45 represents the crank angle resolved NO_x history predicted by the simulation normalized by the ratio of the measured exhaust NO_x concentration to the predicted NO_xconcentration. The incylinder NO_x histories are measured by total cylinder sampling. The engine conditions are shown in table 11.

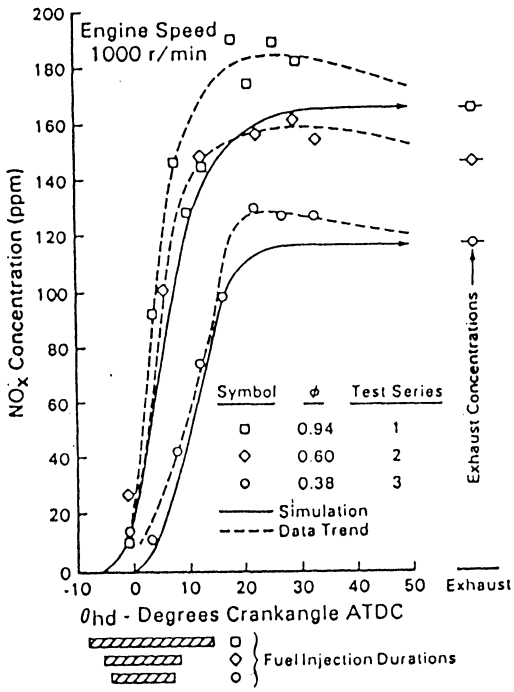

Fig. 43. Measured and simulated total–cylinder averaged NO_x concentration histories at various equivalence ratios, ϕ. No simulation was done at ϕ=0.6.

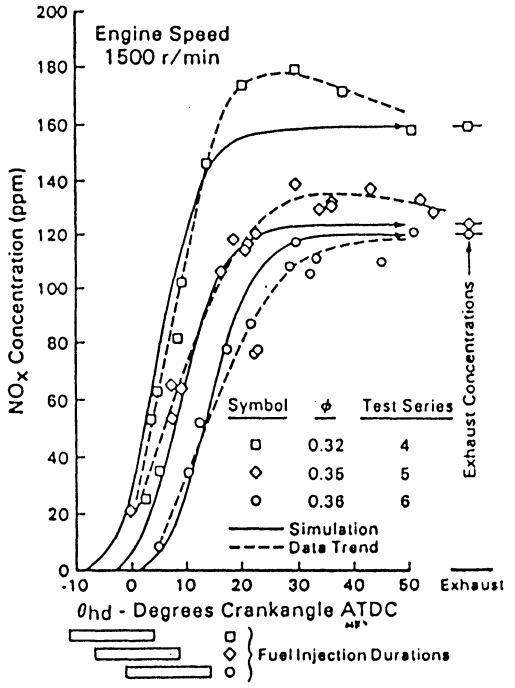

Fig. 44. Measured and simulated total–cylinder averaged NO_x concentration histories at 1500 RPM, lightload at various fuel–injection timings.

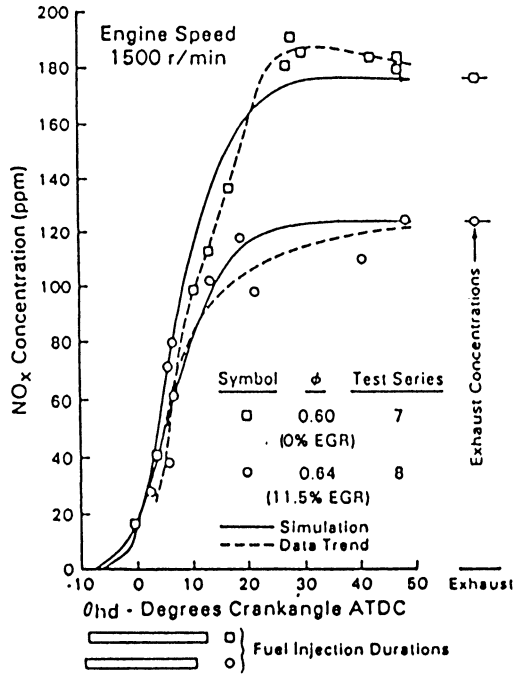

Fig. 45. Measured and simulated total–cylinder averaged NO_x concentration histories at 1500 RPM and medium load conditions, with and without EGR.

Table 11. Engine test conditions.

Test series	Engine speed (r/min)	Equivalence ratio-overall (0_{ov})	EGR (%)	Injection timing (°BTDC)	Injection duration (°CA)	Fuel per cycle (mg)	Exhaust NO_x concentration[b] Experiment (ppm)	Model (ppm)
1	1000	0.94	0	8.5	22.8	36.8	166 ± 2[c]	322
2	1000	0.60	0	5.5	13.4	22.8	148 ± 3	(a)
3	1000	0.38	0	4.5	11.5	15.3	117 ± 8	197
4	1500	0.32	0	12.5	15.3	14.7	160 ± 4	257
5	1500	0.35	0	7.7	15.3	16.0	125 ± 7	172
6	1500	0.36	0	2.1	15.2	16.4	120 ± 6	102
7	1500	0.60	0	8.9	21.3	27.5	177 ± 3	249
8	1500	0.64	11.5	9.2	19.7	26.9	124 ± 6	99

For all tests: Intake Air Temperature—299 K; Intake Air Pressure—0.962 Atm; Initial Oil and Water Temperature—360 K.

[a]Dumping data only. No simulations were run for these conditions.

[b]Dry volumetric basis.

[c]Standard deviation.

TURBULENT MIXING CORRELATIONS

Lipkea and DeJoode [36] have developed a model for a direct injection diesel engine. The general idea that a fuel jet behaves like a jet of pure gas is used to model one fuel jet and then they assume no interaction between jets. The fuel injected is divided into equal discrete mass elements, each one forming a zone which entrains and moves. All the air outside the jet zones is considerd as one unburned zone. The atomization and vaporization are assumed to

be faster than the mixing and are not modelled. The concentration and movement of the zones are based on fully developed turbulent mixing correlations. The model takes into account the internal recirculation within the fuel jet and the effect of swirling flow upon the free jet. Transition to a wall jet is allowed. The combustion chamber is treated as a cylinder with the same diameter as the bowl. The relations used to calculate cylinder pressure, local temperature and composition of each burning zone and the unburned zone are:

the fuel stoichiometri
conservation of mass
ideal gas equation of state
first law of thermodynamics
heat transfer out of the cylinder
a simple air and fuel global kinetics scheme
the Zeldovich mechanism and
a property model (variable specific heats).

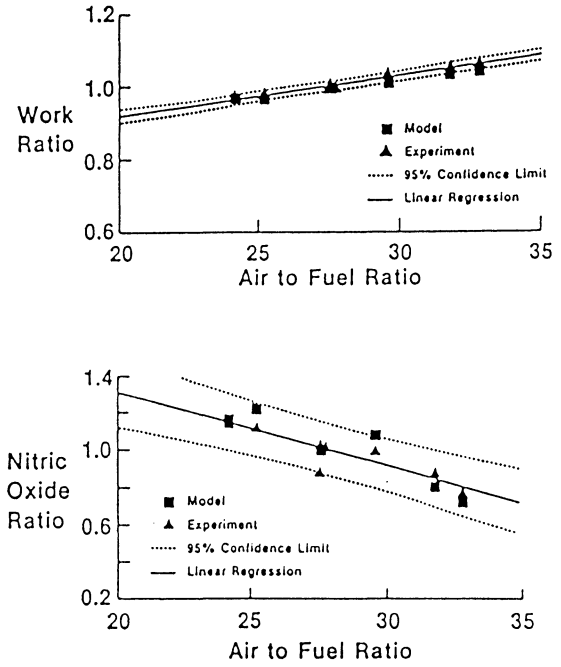

Fig. 46. Comparision of the model and experimental results for indicated work ratio and nitric oxide ratio versus air–to–fuel ratio at constant intake pressure at 2500 rpm and full load for the engine configuration specified in table 13.

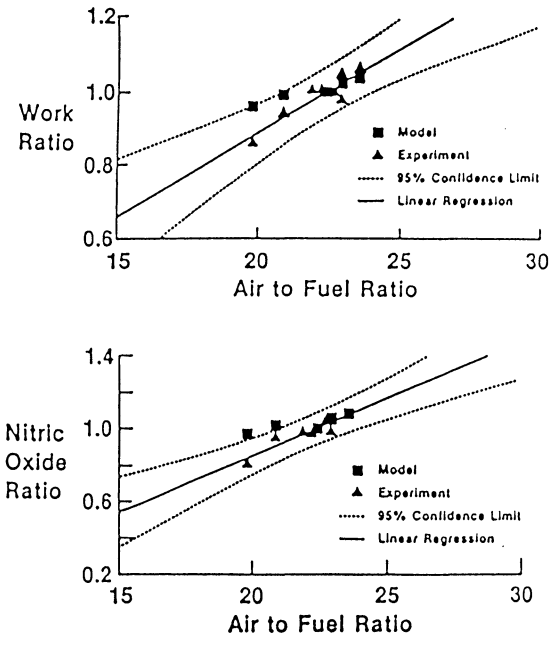

Fig. 47. Comparison of the model and experimental results for indicated work–ratio and nitric oxide ratio versus air–to–fuel ratio at constant intake pressure at 1500 rpm and full load for for the engine configuration specified in table 13.

It is assumed that during each time interval the pressure is the same everywhere in the cylinder and that the composition and temperature of each zone are uniform. Thermodynamic equilibrium is reached at the end of each time interval in each zone. The model requires the pressure and mass in the cylinder at intake valve closure and an estimate of the metal surface temperature as input data. The temperature in the chamber is assumed to be uniform until fuel injection begins. The model is assumed to be valid for the direct–injection diesel engine configurations and conditions given in table 12. Figs 46 – 49 show comparisions between measured and predicted values; the engine configuration is given in table 13. The air–to–fuel ratio is varied by varying the intake air temperature. Lipkea et al. [37] have used the model described above to study the effects of several parameters. The parameters are given in table 14. They came to the conclusion that a "one at a time " parametric study can not give the optimum engine.

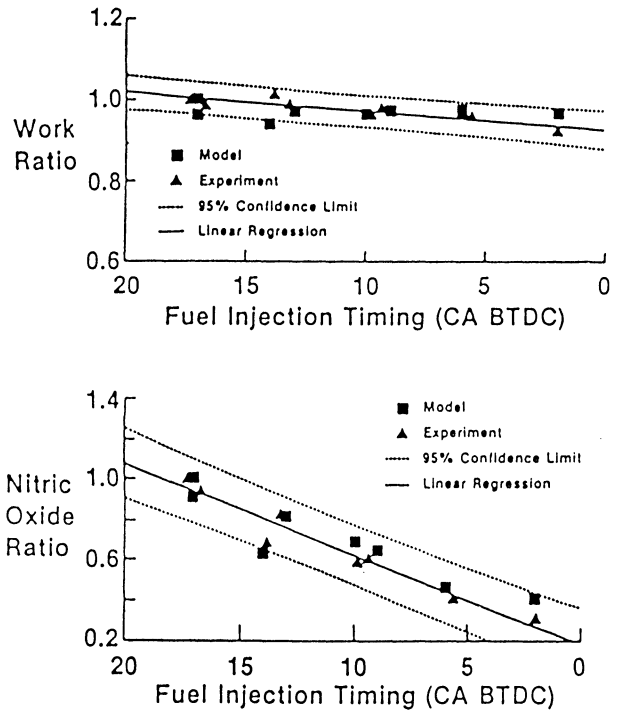

Fig. 48. Comparision of the model and experimental results for indicated work ratio and nitric oxide ratio versus fuel injection timing at 1500 rpm and full load for the engine configuration specified in table 13.

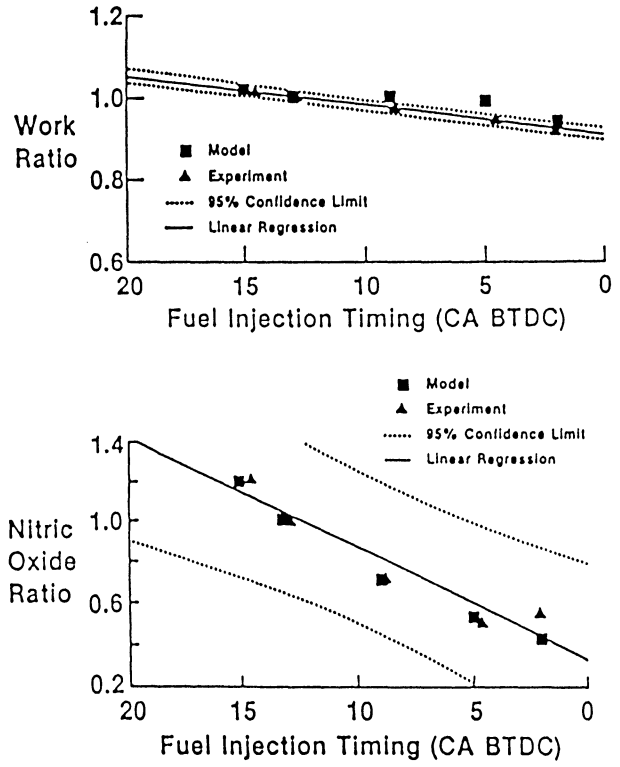

Fig. 49. Comparison of the model and experimental results for indicated work ratio and nitric oxide ratio versus fuel injection timing at 2500 rpm and full load for the engine configuration specified in table 13.

Table 12. Representative engine configurations and operating conditions.

Bore (mm)	90 - 140
Displacement (L)	2 - 16
Power (kW)	30 - 400
Speed (rev/min)	1000 - 2500

Table 13. Engine configuration.

Bore (mm)	106.5
Stroke (mm)	110.0
Connecting Rod Length (mm)	181.0
Compression Ratio	18.0
Combustion Bowl Radius (mm)	29.3
Swirl Ratio	2.0
Fuel Injection Nozzle	
Number of Nozzle Holes	4
Nozzle Hole Diameter (mm)	0.295

Table 14. Parameters varied.

Design Parameters	Abbreviation
Fuel injection nozzle:	
Number of holes	HOLE#
Diameter of hole	DIAHOL
End of induction swirl ratio*	SWIRL
Compression ratio	CRAT
Fuel quantity (fuel and air ratio)	FMASS
Fuel injection timing and duration:	
Timing (fixed duration)	TIMING
Duration (fixed start/vary end)	INJEND
Duration (fixed end/vary start)	INJSTR
In-cylinder conditions at intake valve closure	
Air mass (fuel and air ratio)	AIRMAS
Pressure	PRESS
Engine speed	ERPM
Combustion bowl (diameter)	BWLDIA

* Air charge rotational speed (rev/min) at the end of induction divided by the engine speed (rev/min).

3:3:4 MULTIDIMENSIONAL MODELS

Multidimensional models are based on the numerical solution of governing coupled partial differential equations solved in fine geometric grids with two or three dimensions in the combustion chamber. They are limited by the inadequacy of submodels for turbulence, combustion chemistry etc, and by computer size and cost of operation. Multidimensional models are presented in [26,27,28].

4 DISCUSSION AND CONCLUSION

As can be seen in fig. 11 the only NO formation process, if any, considered is the Zeldovich or the extended Zeldovich mechanism. This is because of the high temperatures in the diesel combustion process. Prompt and fuel NO contribute about 100 ppm each while NO_x exhaust from a diesel engine constitutes about 1000 ppm. See also table 1 concerning prompt NO in diesel engines. All models assume the reaction rates of O, O_2 and N_2 to be fast enough to assume equilibrium concentrations of O, O_2 and N_2.

On page 46 the models are tabulated together with a an indication of how good the predictions are, experimental data needed for each prediction and then possibilty of changing engine geometry etc.

4:1 REGRESSION MODELS

The agreement between predicted and experimental values in a regression model within the interval in which the model is constructed is (hopefully) good. For each prediction, independent variables are needed as input data, in this case the transient test cycle for speed and load. In order to construct a model, several experimental results are required, in this case speed and load cycles and NO_x emissions. If for example, the engine geometry is changed the constants in eq. (23) have to be fitted with new experimental data. The model is also used to predict particulate, hydrocarbon and carbon monoxide emissions.

4:2 WELL–STIRRED REACTORS

Both well–stirred reactor models use the temperature as input data either calculated (1) or measured (2).

4:2:1 LUMPED ONE–STEP REACTION

For the model developed by Ahmad et al. and Plee et al. the predicted values seem to lie within $\pm$50 % of the experimental values, as can be seen in figs 14, 15 and 16. For each prediction a P–t diagram is required. The model does not take into account the engine geometry.

4:2:2 EXTENDED ZELDOVICH

Wu and Peterson's model predicts $EINO_x$ to within a tolerance of 25% [18]. To predict

Model	Agreement with expt'l results	Possibility to change engine geom.	Experimental data required
Regr.	Hopefully good	No	Test cycle. For construction much expt'l data are needed
Lumped one–step reaction	±50% figs 14,15 and 16	Does not take engine geometry into account	P–t diagram
Extended Zeldovich	±25%	Does not take engine geometry into account.	Temperature, P–t diagram
Burned–unburned	±20% figs 22 – 25	Determines some constants for changing engine geom.	P–t diagram
Spatial variation	Not good	New standard air measurement.	Standard air measurement
Single–zone	±100% figs 31 – 35	Yes for DI	Fuel inj. press., swirl ratio
No mixing	±200% figs 36 – 38	Yes for both DI and IDI	
Sto–chastic mixing	±10%	Yes for IDI, some calibration is needed.	Expt'l data for calibration. Fuel inj. profile, exhaust pressure
Turbulent mixing correl.	Within 95% conf. lim. of expt	Yes for DI	Data to estimate mass and press. at intake valve closure.

$EINO_x$ they need measured temperature, engine speed and a P–t diagram. The fuel burning rate is calculated from the P–t diagram. The model does not take into account the engine geometry.

4:3 PARTIALLY–STIRRED REACTORS

4:3:1 BURNED UNBURNED ZONE MODELS

From figs 22, 23, 24 and 25 it seems that the experimental results are within $\pm$20 % of the predictions. A P–t diagram is needed for prediction. In order to changes the engine geometry, the constants C_z, B and T_z in eq. (38) have to be redetermined. The model has not been tested on a real diesel engine.

4:3:2 SPATIAL VARIATIONS

As can be seen in fig. 26 neither β_m, β_ϕ nor β_f is a good prediction for the effects of EGR. Standard air NO_x measurements are required. The model predicts $[NO_x]/[NO_x]_{sd}$.

4:3:3 PHENOMENOLOGICAL MODELS

In phenomenological models the engine geometry is approximated by, for example, a cylinder with the same diameter as the bowl.

SINGLE–ZONE

The single–zone model developed by Dent et al. predicts the NO exhaust to within $\pm$ 100% as can be seen in figs 31 – 35. Fuel injection pressure diagram and swirl ratio at inlet valve closure are needed as input data. Several parameters such as engine dimensions and operating conditions, can be changed. The model has been developed for a DI diesel engine at the University of Technology, Loughborough England. Allowance is made for the angle of the spray axis relative to the cylinder head.

MULTIZONE– NO MIXING

In figs 38, 39 and 40 the experimental NO_x concentration lies within $\pm$ 200% of the prediction made by the model developed by Hiroyasu et al. The model is valid for both DI and IDI diesel engines and is sensitive to many parameters but not to the angle between the spray axis and the cylinder. The model was developed at the University of Hiroshima. The

computation was carried out in only 18 of the 250 packages to save time. These 18 packages were chosen to represent typical packages. The computation takes 4 minutes on a HITAC M–180 computer. A program for the injection simulation [41] is used to calculate the history of the injection pressure, the nozzle needle lift, the injection rate of fuel etc. for the design parameters and the operatings condition in an engine. This is used as input data for the model.

MULTIZONE–STOICHASTIC MIXING

The model developed by Mansouri et al. predicts the NO_x concentration with only 10 % error [33]. The model is sensitive to many parameters but not to the angle between the spray axis and the cylinder axis. The model was developed for an IDI diesel engine at General Motors and Massachusetts Institute of Technology. Several constants are used for calibration, but these constants do not significantly affect predicted [NO_x]. Exhaust pressure, fuel properties and wall temperatures are needed as input data. As can be seen in figs 43, 44 and 45 the in–cylinder NO_x concentrations given by the model are not higher than the exhaust NO_x concentrations, as is found experimentally.

MULTIZONE–TURBULENT MIXING CORRELATIONS

The model presented last in this paper is that developed by Lipkea and DeJoode and gives predictions within the 95 % confidence limit of experimental data. It requires experimental data to estimate the mass and pressure in the cylinder at intake valve closure. The possibility of changing parameters is good within the specifics of a DI diesel engine. No allowance is made for the angle between spray axis and cylinder head. The model was developed at John Deere and a single run takes 5 CPU seconds on an IBM 3090 computer.

4:4 CONCLUSION

In the regression, well–stirred reactor, burned–unburned and spatial variations models not many parameters can be varied. Models which are worth further investigation are the phenomenological models. Unfortunately, not much information is available on the last presented model since it was developed at the John Deere company. The single–zone model and the multizone model with no mixing do not show as good agreement with experimental data as the multizone model with stochastic mixing. On the other hand, the stochastic mixing model uses eight constants which have to be determined by experiment. Multidimensional models are not yet good enough for realistic use.

5 MEANS OF DECREASING NO_x EXHAUST

Almost all NO is formed within 20° CA after the start of combustion [35]. In an IDI diesel engine most NO is formed in the prechamber and is transported to the main chamber [34]. See fig. 50.

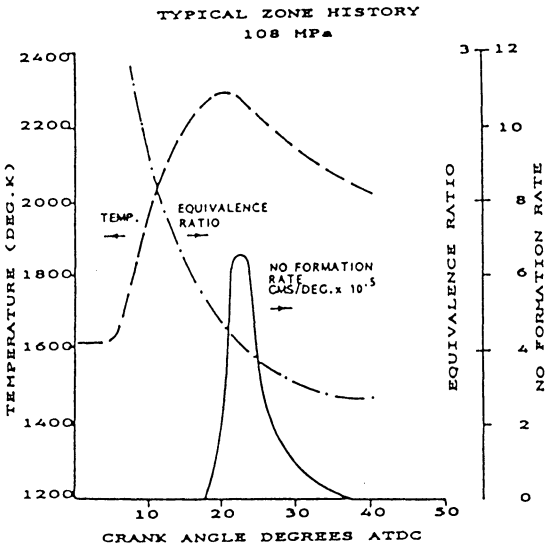

Fig. 50. Mixing, temperature and nitric oxide formation history in a typical combustion zone under moderate injection pressure conditions.

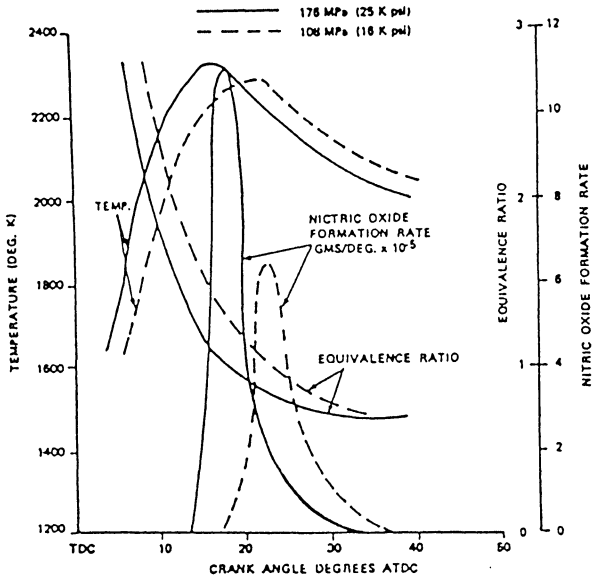

Fig. 51. Temperature equivalence ratio, and nitric oxide formation rate in a typical combustion zone with different injection pressures.

The NO_x formation rate is sensitive to many parameters. Increased pressure gives an increased rate of NO formation. The NO formation rate increases with advanced injection timing due to changes in local temperature and local [O] [52]. But as we can see in fig. 51, injection retardation with high injection pressure causes higher local temperatures, so the NO formation rate increases. As can be seen in fig. 52 the NO formation rate decreaseing with decreased ignition delay. Increased fuel and air mixing increases NO_x [45, 46]. The NO formation rate is very sensitive to the temperature. The best way to decrease NO_x is to lower local temperatures without retarding the combustion process or increasing the combustion duration. This can be done with exhaust gas reciculation or in turbo–charged engines by cooling the intake charge [42, 43]. By combining EGR and intake air throttling, the air–to–fuel ratio is controlled [47] and thus the NO formation rate.

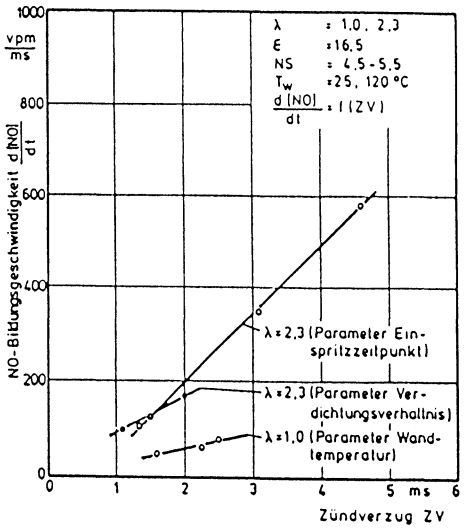

Fig. 52. NO formation rate versus ignition delay.

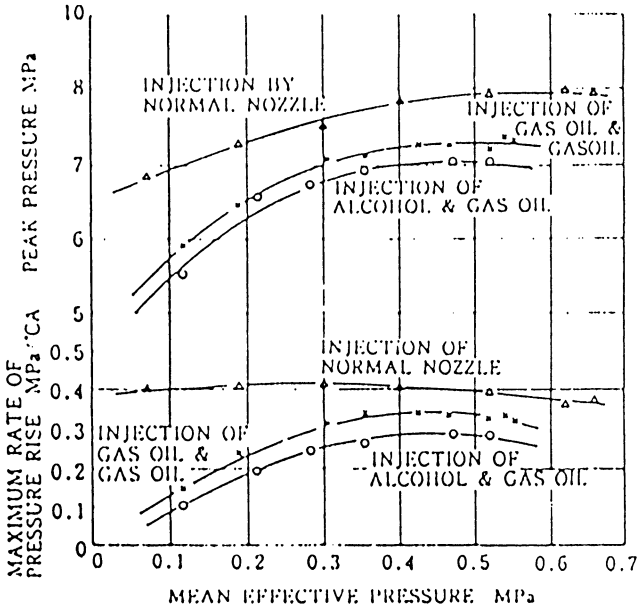

Fig. 53. Comparision of maximum pressure and maximum rate of pressure rise for a normal injector and the dual fuel injector.

Using a dual fuel injector two different kinds of fuel can be injected; for example, alcohol and gas oil reduce NO_x, fig. 53. Goto and Kontani [48] have developed such an injector. Another way to reduce NO_x emissions is to use an emulsion of water in dieseloil as fuel. There are still some problems to be solved in the construction of an emulsifier that can be used in real life. When engines with conventional mechanical systems have reached the end of their capabilities, electronic diesel control could be useful. This type of system controls the start of injection and quantity of fuel injected [50].

Hales and May [51] came to the conclusion that turbo–charged and aftercooled versions of direct–injection engines with high injection pressures and turbo–charged swirl chamber engines are best suited to meet more stringent emission standards. In the future particulate traps will also be necessary.

ACKNOWLEDGEMENTS

Firstly, I would like to thank my supervisors, Göran Holmstedt at the Department of Physics in Lund and Jan Olof Larsson and Tommy Bertilsson at the Scania division of Saab–Scania in Södertälje without whose patience and help I could not have managed. I am also grateful to Göran Olsson and Per Cederbalk at the Department of Physics and Ann Bruhn and Maria Andersen at the Department of Fire Safety Engineering in Lund.

REFERENCES

1. Caretto L.S: Mathematical Modeling of Pollutant Formation, Progress in Energy and Combustion Science Vol. 1 (1976)
2. Glassman I: Combustion (1977)
3. Hayhurst A.N. and Vince I.M: Nitric Oxide Formation from N_2 in Flames: The Importance of Prompt NO. Progress in...Vol 6 Nr 1 (80)
4. Sawyer R.F: The Formation and Destruction of Pollutants in Combustion Processes: Clearing the Air on the Role of Combustion Research. Eighteenth symposium (international) on Combustion (1981)
5. Pershin D.W, Cichanowicz J.E, England G.C, Heap M.P,and Martin G.B: The Influence of Fuel Composition and Flame Temperature on the Formation of Thermal and Fuel NO_x in Residual Oil Flames. 17th symp on Comb. p 724 (1979)
6. Baulch D.L. et al: Evaluated Kinetic Data for High Temperature Reactions. Vol 2 CRC Press(1975)
7. Sawyer R.F, Cernansky N.P. and Oppenheim A.K: Factors Controlling Pollution Emissions from Gas Turbines. Atmospheric Pollution by Aircraft Engines, Chapter 22, 41st Meeting of the AGARD Propulsion and Energetics Panel, London 1973
8. De Soete G.G: Overall Rates of NO and N_2 Formation from Fuel Nitrogen. Fifteenth Symp. on Comb. (1975)
9. Fenimore C.P. Thirteenth Symp. on Comb. (1971)
10. Bachmaier F, Eberius K.H. and Just T: Combustion Science and Technology 7,77 (1973)
11. Appleton J.P and Heywood J.B: The effects of Imperfect Fuel–Air Mixing in a Burner on NO Formation from Nitrogen in the Air and the Fuel. 14th Symp.on Comb. p 780 (1973)
12. Thompson D, Brown T.D. and Beer J.M: NO_x Formation in Combustion. Combustion and Flame, 19, 69–79, (1972)
13. Westenberg A.A: Combustion Science and Technology 4,59 (1971)
14. Schefer R.W. and Sawyer R.F: Lean Premixed Recirculating Flow Combustion for Control of Oxides of Nitrogen. 16th Symp. on Comb, 119–134, (1977)
15. Callahan T.J, Ryan T.W.III, Dietzmann H. and Waytulonis R:The Effects of Discrete Transients in Speed and Load on Diesel Engine Exhaust Emissions. SAE paper 850109
16. Ahmad T. and Plee S.L: Application of Flame Temperature Correlations to Emissions from a Direct–Injection Diesel Engine, SAE special publications 831734
17. Plee S.L, Ahmad T. and Myers J.P: Diesel NO_x Emissions – A Simple Correlation Technique for Intake Air Effects, Nineteenth Symposium (international) on Combustion, pp 1495–1502 (1983)

18. Wu K–J and Peterson R.C: Correlation of Nitric Oxide Emission from a Diesel Engine with Measured Temperature and Burning Rate, SAE Paper No 861566
19. Wu K–J and Peterson R C: Effects of Flame Temperature and Burning Rate on Nitric Oxide Emission from a Divided Chamber Diesel Engine, Twentyfirst Symposium (International) on Combustion 1986 pp 1149–1157
20. Peterson R.C. and Wu K–J: The Effect of Operating Conditions on the Flame Temperature in a Diesel Engine, SAE Paper No 861565,1986
21. Plee S.L. and Ahmad T: Relative Roles of Premixed and Diffusion Burning in Diesel Combustion, SAE Transactions, Vol 92, pp 4892–4909, 1983
22. Cakir H: Nitric Oxide formation in Diesel engines, Inst Mech Eng (Lond) Proc v 188 n 46, 1974 pp 477–483
23. Ikegami M, Kawai E. and Kihara Y: Reducing Oxides of Nitrogen in a Diesel Engine by Means of Exhaust Gas Recirculation. Bulletin of JSAE n 6 April 1974 pp 65–74
24. Hiroyasu H: Diesel Engine Combustion and its Modeling. JSME, SAEJ, MESJ Diagnostics and Modeling of Combustion in Reciprocating Engines, Symposium Tokyo September 1985 pp 53–75
25. Henein N. A: Analysis of Pollutant Formation and Control and Fuel Economy in Diesel Engines, Progress in Energy and Combustion Science, Vol 1 pp 165–207,1976
26. Butler T. D, Cloutman L. D, Dukowicz J. K, Ramshaw J. D and Krieger R. B: Toward a Comprehensive Model for Combustion in a Direct–Injection Stratified–Charged Engines, Combustion Modeling in Reciprocating Engines, Ed. by Mattavi J. N. and Amann C. A, Plenum press 1980, 231
27. Gosman A. D, Johns R. J. R. and Watkins A. P: Development of Prediction Methods for in cylinder Processes in Reciprocating Engines, Combustion Modeling in Reciprocating Engines, Ed by Mattavi J. N. and Amann C. A, Plenum press 1980, 69
28. Diwakar R: Multidimensional Modeling Applied to the Direct–Injection Stratified–Charged Engine, Calculation Versus Experiment, SAE paper No 810222,1981
29. Hiroyasu H, Kadota T. and Arai M: Development and Use of a Spray Combustion Modeling to Predict Diesel Engine Efficiency and Pollutant Emissions, Part 1, Combustion Modeling. Bulletin of the JSME vol 26 No 214–12, April 1983
30. Hiroyasu H, Yoshimatsu A. and Arai M: Mathematical Model for Predicting the Rate of Heat Release and Exhaust Emissions in IDI Diesel Engines. Diesel Engines for Passenger Cars and Light Duty Vehicles, I Mech E Conf 1982–8
31. Hiroyasu H, Furukawa O, Arai M, Iida S. and Motonaga H: Development and Use of a Spray Combustion Modeling to Predict Diesel Engine Efficency and Pollutant Emissions Part 3. An Analysis by the Method of System–model Transformation, Bulletin of the JSME Vol 26 No 214–14, April 1983

32. Hiroyasu H, Kadota T. and Arai M: Development and Use of a Spray Combustion Modeling to Predict Diesel Engine Efficiency and Pollutant Emissions Part 2. Computational Procedure and Parametric Study, Bulletin of the JSME Vol 26 No 214–13, April 1983
33. Mansouri S. H, Heywood J. B and Radhakrishnan K: Divided Chamber Diesel Engine part 1. A cycle Simulation which Predicts Performance and Emissions, SAE paper No 820273
34. Mansouri S. H, Heywood J. B and Ekchian J. A: Studies of NO_x and Soot Emissions from an IDI diesel Engine Using an Engine Cycle Simulation. Diesel Engines for Passenger Cars and Light duty Vehicles, I Mech E Conf 1982–8
35. Liu X. J, Siegla D. and Kittelson D. B: In–Cylinder NO_x Histories in an Indirect Injection Diesel Engine: Comparision between Experimental Data and Model Predictions, Twentieth Symposium (International) on combustion 1984 pp 45–52
36. Lipkea W. H. and DeJoode A. D: A Model of a Direct Injection Diesel Combustion System for Use in Cycle Simulation and Optimization Studies, SAE paper No 870573
37. Lipkea W. H, DeJoode A. P and Christenson S. R: The Relationship Between Nitric Oxide and Work as Influenced by Engine Operating Conditions and Combustion System Parameters for a Direct Injection Diesel Engine, SAE paper No 870269
38. Dent J. C. and Mehta P. S: Phenomenological Combustion Model for a Quiscent Chamber Diesel Engine, SAE paper No 811235
39. Kyriakides S. C, Dent J. C. and Mehta P. S: Phenomenological Diesel Combustion Model Including Smoke and NO Emission, SAE paper No 860330
40. Dent J. C, Mehta P. S. and Swan J: A Predictive Model for Automotive DI Diesel Engine Performance and Smoke Emissions, IMechE conference "Diesel engines for passenger cars and light duty vehicles", London 1982
41. Hiroyasu H. and Matsunari F. Trans. JSME, 34–260 (1968), 755
42. Shahed S.M: The role of Fuel–Air Mixing in Diesel Combustion and Emissions. ASME, Fluids Engineering Division, International Symp. on Flows in Internal Combustion Engines–III vol 28 1985 p 159–164
43. Plee S.L, Ahmad T. and Myers J.P: Flame Temperature Correlation on Diesel Particulate and NO_x Emissions. SAE paper No 811195
44. Kleine H: Geschwindigkeit der Stickoxidbildung im Dieselproceβ mit direkter Einspritzung. MTZ Motortech Z v 38 n 9 sep 1977 p 399–400, 403–404, 407–408
45. Khan I.M, Greeves G. and Probert D.M: Prediction of Soot and Nitric Oxide Concentrations in Diesel Exhaust, Instn Mech Engrs Conference on Air Pollution Control in Transport Engines, Paper C142/71 pp 205–217
46. Bertoli C, Corcione F.E, Police G. and Valentino G: Effect of Combustion Chamber

Shape on Air Flow Field in a D.I. Diesel Engine. SAE paper No 870338

47. Shogren V.L, Takeuchi K. and Hara H: Emission Controls for a 2.2L Diesel Engine. SAE paper No 860417
48. Goto S. and Kontani K: A Dual Fuel Injector for Diesel Engines. SAE paper No 851584
49. Hsu B.D: Combustion of Water–in–Diesel Emulsion in an Experimental Medium Speed Diesel Engine. SAE paper No 860300
50. Gaschler E: Exhaust Emissions Influenced by Electronic Diesel Control, SAE paper No 860142
51. Hales J.M. and May M.P: Transient Cycle Emissions Reduction at Ricardo – 1988 and Beyond, SAE paper No 860456
52. Khan I.M. and Wang C.H.T: Factors Affecting Emissions of Smoke and Gaseous Pollutants from Direct Injection Diesel Engines, Instn.Mech. Engrs Paper C151/71 pp293–303
53. Dent J.C: Turbulent Mixing Rate – Its Effect on Smoke and Hydrocarbon Emissions from Diesel Engines, SAE paper 800092
54. Gardiner: Combustion Chemistry
55. Baulch D.L, Drysdale D.D. and Llooyd A.C: Critical Evaluation of Rate Data for Homogeneous, Gas Phase Reactions of Interest in High Temperature Systems, Nos. 1 and 2, Departement of Phys. Chem., The University of Leeds, England, 1968.
56. Matsuoka S. Kamimoto T. Matsui Y. and Aoagi (J) Y: An Introduction to the Research on Combustion Mechanism and Formation–Extinction Processes of NO_x and Soot–Particulate in a Direct Injection Diesel Engine. VDI–Berichte Nr. 370, 1980
57. Aoyagi Y. Takeyuki K. Matsui Y. and Matsuoka S: A Gas Sampling Study on the Formation Processes of Soot and NO in a DI Diesel Engine. SAE Paper No 800254
58. Billick I.H. and Gaynor A.J: The Measurement of NO_2 from Gas Flames. Combustion and Flame 71: 331–335 (1988)
59. Cernej A. and Dobovisek Z: The effect of Bound Nitrogen on Diesel Engine NO_x–Emission, VDI–Berichte Nr. 370, 1980
60. Harris G.W, Mackay G.I, Iguchi T, Schiff H.I. and Schuetzle D.: Measurement of NO_2 and HNO_3 in Diesel Exhaust Gas by Tunable Diode Laser Absorption Spectrometry, Environ. Sci. Technol., Vol. 21, No. 3, 1987
61. de Soete G: De verschillende parameters welke een invloed hebben op de stikstofoxidevorming bij benzine– en dieselmotoren, alsso de kontroletechnieken. Ingenieursblad v 43 n 10 May 16 1974 p 322–333
62. Barsic N.J: Variability of Heavy–Duty Diesel Engine Emissions for Transient and 13 – Mode Steady – State Test Methods. SAE paper no 840346
63. Levy A: Unresolved problems in SO_x No_x Soot Control in Combustion. Nineteenth

Symposium (international) on Combustion.

64. Barbella A, Ciaiolo A, Belardini P, Bertoli C. and Police G: Behavior of DI and IDI Diesel Engines Burning Low Quality Fuels. C333/87 IMechE 1987
65. Derwent R.G. and Hough A.M: Modelling Secondary Pollutants from Motor Vehicles and Their Control. C330/87 IMechE 1987
66. Waters M.H.L: The Fuel Consumption of Diesel and Petrol Cars and Light Vans of Similar Road Performance. C106/82
67. Flechon P: XX FISITA Congress. The Automotive Future. SAE P–143
68. Cartellieri W.P. and Wachter W.F: Status Report on a Preliminary Survey of Strategies to Meet US – 1991 HD Diesel ERmission Standards Without exhaust Gas Aftertreatment. SAE paper no 870342
69. Afify E.M, Korah N.S. and Dickey D.W: The Effect of Air Charge Temperature on Performance, Ignition Delay and Exhaust Emissions of Diesel Engines Using W/O Emulsion as Fuel, SAE paper no. 870555
70. Reitz R.D: Comparisions of Computed and Measured Premixed Charge Engine Combustion, Combustion and Flame 60: 309–322 (1985)
71. Yoshida E, Nomura H. and Sekimoto M: Fuel and Engine Effects on Diesel Exhaust Emissions. SAE paper no.860619
72. Henningsen S: Evaluation of Emissions and Heat–Release Characteristics from a Simulated Low–Heat Rejection Diesel Engine. SAE paper no 871616
73. Shimoda M. Suzuki T. and Shigemori M: Observation of the Particulate Formation Process in the Cylinder of a Direct Injection Diesel Engine. SAE paper no.870268